

**Pharmacokinetics Modeling and Molecular Modeling of Drug-Drug Interactions  
Between Opioids and Benzodiazepines**

by

**Beihong Ji**

Bachelor of Science, China Pharmaceutical University, 2017

Submitted to the Graduate Faculty of  
School of Pharmacy in partial fulfillment  
of the requirements for the degree of  
Master of Science

University of Pittsburgh

2019

UNIVERSITY OF PITTSBURGH  
SCHOOL OF PHARMACY

This thesis/dissertation was presented

by

**Beihong Ji**

It was defended on

April 2, 2019

and approved by

Junmei Wang, Associate Professor, Pharmaceutical Sciences

Sameul M. Poloyac, Professor, Pharmaceutical Sciences

Xiang-Qun Xie, Professor, Pharmaceutical Sciences

Lirong Wang, Assistant Professor, Pharmaceutical Sciences

Zhiwei Feng, Assistant Professor, Pharmaceutical Sciences

[Thesis Advisor/Dissertation Director]: Junmei Wang, Associate Professor,  
Pharmaceutical Sciences

Copyright © by Beihong Ji

2019

# **Pharmacokinetics Modeling and Molecular Modeling of Drug-Drug Interaction Between opioids and benzodiazepines**

Beihong Ji, B.S

University of Pittsburgh, 2019

## Abstract

The potential drug-drug interactions (DDIs) of concurrent use of opioids and benzodiazepines have aroused high attention in the world for the severe side effects when two types of drugs are co-administered. However, there is much unknown in the DDI between these two kinds of drugs. The objective of this project is to find out the mechanism underlying the DDIs between opioids and benzodiazepines. There are two basic factors can contribute to the interactions, pharmacokinetic (PK) interaction and pharmacodynamic (PD) interaction. PK interaction is one of the most common reasons that lead to DDI. This kind of interaction may occur when two drugs are metabolized by the same Cytochrome P450 enzymes. In this work, we quantitatively predicted the DDI between oxycodone and diazepam through empirical PK modeling, minimal physiologically-based PK (PBPK) modeling and full PBPK modeling. Another possibility causing the DDI is PD interaction. In PD study, we used molecular modeling techniques including molecular docking, molecular dynamics simulations and MM/PBSA calculations to predict the pharmacodynamic interaction between opioids and benzodiazepines. The results of PK interaction study indicated that benzodiazepines have limited inhibitory effect on opioids and the extent of inhibition slightly increased with the overdose of benzodiazepines. Usually PK interactions might only be observed when highly increasing the dosage of benzodiazepines. The results of PD interaction study indicated that benzodiazepines may act as agonists or antagonists of the  $\mu$ - and  $\kappa$ -opioid receptors. We concluded that PD interaction is likely to play a more important role in DDIs between opioids and benzodiazepines.

Key words: opioid, benzodiazepine, drug-drug interaction, PK, PBPK, molecular modeling

## Table of Contents

<b>PREFACE</b> .....	<b>xi</b>
<b>1.0 INTRODUCTION</b> .....	<b>1</b>
<b>1.1 DRUG ABUSE OF OPIOIDS AND BENZODIAZEPINES</b> .....	<b>1</b>
<b>1.2 OXYCODONE</b> .....	<b>2</b>
<b>1.3 DIAZEPAM</b> .....	<b>4</b>
<b>1.4 DDI MECHANISM</b> .....	<b>6</b>
<b>2.0 METHODS</b> .....	<b>8</b>
<b>2.1 PHARMACOKINETICS</b> .....	<b>8</b>
<b>2.1.1 Empirical PK modeling</b> .....	<b>8</b>
<b>2.1.2 Full PK modeling</b> .....	<b>11</b>
<b>2.1.3 Minimal PK modeling</b> .....	<b>14</b>
<b>2.2 PHARMACOKINETICS</b> .....	<b>17</b>
<b>2.2.1 Molecular docking</b> .....	<b>18</b>
<b>2.2.2 Molecular dynamics simulations</b> .....	<b>19</b>
<b>2.2.3 MM/PBSA calculations</b> .....	<b>20</b>
<b>3.0 RESULTS</b> .....	<b>21</b>
<b>3.1 PHARMACOKINETICS</b> .....	<b>21</b>
<b>3.1.1 Empirical PK modeling</b> .....	<b>21</b>
<b>3.1.2 Full PK modeling</b> .....	<b>28</b>
<b>3.1.2.1 Competitive inhibition</b> .....	<b>30</b>

3.1.2.2 Mixed type inhibition .....	35
3.1.2.3 Mixed type inhibition .....	37
3.1.3 Minimal PK modeling.....	45
3.2 PHARMACODYNAMICS .....	53
3.2.1 Molecular docking.....	53
3.2.2 Molecular dynamics simulation .....	58
3.2.3 MM/PBSA calculations.....	62
4.0 SUMMARY AND CONCLUSIONS .....	70
4.1 PHARMACOKINETICS.....	70
4.2 PHARMACODYNAMICS .....	70
APPENDIX .....	71
BIBLIOGRAPHY .....	76

## List of Tables

Table 1 The docking scores and calculated $K_i$ for oxycodone and diazepam when binding to CYP3A4.....	14
Table 2 Parameters used in empirical PK modeling.....	24
Table 3 AUC ratios when using OXY and different dose of DZP together in PySB.....	25
Table 4 The AUC, $C_{max}$ and $T_{max}$ of 30 mg PO OXY, 10 mg PO DZP and 1 mg/kg DZP. ....	29
Table 5 The AUC Ratio and $C_{max}$ Ratio of the DDI profiles for PO OXY and 10 mg, 100 mg and 500 mg and 1000 mg of PO/IV DZP. ....	31
Table 6 The AUC Ratio and $C_{max}$ Ratio of the DDI profiles for PO OXY and 10 mg, 100 mg and 500 mg and 1000 mg of PO DZP when applying mixed-type inhibition to the DDI model.....	36
Table 7 The AUC <sub>0-24h</sub> , $C_{max}$ and $T_{max}$ of 4 mg PO buprenorphine, 0.1 mg/kg mg PO fentanyl, 2 mg PO alprazolam, 15 mg PO midazolam and 0.25 mg PO triazolam. ....	38
Table 8 The AUC Ratio and $C_{max}$ Ratio of the DDI profiles for normal dosage of opioids, including oxycodone (30 mg), buprenorphine (4 mg) and fentanyl (0.1 mg/kg) and benzodiazepines, including alprazolam, diazepam, midazolam and triazolam with normal (10 mg) and overdose (1000 mg), respectively. ....	40
Table 9 The AUC <sub>0-24h</sub> Ratio and $C_{max}$ Ratio of 30 mg OXY with the co-administration of 200 mg PO DZP (toxicity dosage).....	44
Table 10 The simulated AUC, $C_{max}$ and $T_{max}$ of 30 mg PO OXY and 10 mg PO DZP. ....	49

Table 11 The AUC Ratio and $C_{max}$ Ratio of the DDI profiles for PO OXY and 10 mg, 100 mg and 500 mg and 1000 mg of PO DZP when applying minimal PBPK model using Simbiology to construct the DDI model. ....	51
Table 12 The docking results (kcal/mol) for opioids and benzodiazepines binding to both the active and inactive X-ray structures of MOR and KOR.....	55
Table 13 Calculated binding free energies (kcal/mol) for individual terms using the MM/PBSA method.....	65
Table 14 The correlation coefficients between calculated binding free energies and different components of energies.....	67
Table 15 The experimental $K_i$ values ( $\mu$ M) as well as the experimental and calculated binding free energies (kcal/mol) (Exp energy and Calc energy) for opioids. ....	67

## List of Figures

Figure 1 The metabolic path ways of oxycodone. ....	4
Figure 2 The metabolic pathways of diazepam. ....	5
Figure 3 Empirical PK model. ....	10
Figure 4 The PBPK model (left panel) and ADAM model (right panel). ....	13
Figure 5 The docking poses of oxycodone and diazepam in CYP3A4. ....	14
Figure 6 The minimal PBPK model.....	16
Figure 7 The Concentration-Time curves of 40 mg OXY co-administered with 10 mg, 20 mg, 50 mg, and 100 mg DZP from PySB. ....	25
Figure 8 The concentration of OXY in empirical PK model predicted by PySB and Simbiology. ....	28
Figure 9 The predicted concentration profiles of 30 mg PO OXY, 10 mg PO DZP and 1 mg/kg IV DZP and their observed data respectively. ....	30
Figure 10 The predicted concentration profiles of 30 mg oxycodone co-administered with 10 mg, 100 mg, 500 mg and 1000 mg DZP.....	32
Figure 11 The AUC <sub>0-24h</sub> Ratio of 30 mg OXY with the presence of 10 mg, 100 mg, 500 mg and 1000 mg of PO/IV DZP. ....	33
Figure 12 The AUC Ratio of OXY with different dosage of PO DZP when K <sub>i</sub> value is ranged in 0.165-165 μM. ....	34
Figure 13 A series of C-T curves of oxycodone in plasma with the presence of 1000 mg diazepam when applying K <sub>i</sub> in range 0.165-165 μM. ....	35

Figure 14 The AUC <sub>0-24h</sub> Ratio of 30 mg OXY with the presence of 10 mg, 100 mg, 500 mg and 1000 mg of PO DZP when applying competitive inhibition and mixed-type inhibition.....	36
Figure 15 The predicted concentration profiles of 4mg Sublingual (SL) buprenorphine, 0.1 mg/kg IV fentanyl, 2 mg PO alprazolam, 15 mg midazolam and 0.25 mg triazolam versus their observed data respectively.....	39
Figure 16 The AUC <sub>0-24h</sub> Ratio of oxycodone, buprenorphine and fentanyl with the presence of normal dose (ND) and overdose (OD) of four benzodiazepines. ....	41
Figure 17 The DDI model between OXY and DZP built using Simbiology.....	46
Figure 18 The predicted concentration profiles of 30 mg PO OXY and 10 mg PO DZP as well as their observed data respectively by Simbiology. ....	49
Figure 19 The predicted concentration profiles of 30 mg oxycodone co-administered before and after 10 mg, 100 mg, 500 mg and 1000 mg DZP by Simbiology.....	50
Figure 20 The correlation between AUC Ratio of OXY when simultaneously taking with different dose of DZP obtained from Simcyp and Simbiology. ....	51
Figure 21 The docking poses of opioids and benzodiazepines with opioid receptors.....	56
Figure 22 The RMSD results in the MD trajectories of MOR and KOR system. ....	60
Figure 23 The comparison of the crystal structure (in grey) with the MD structure (in orange (opioids) and in purple (benzodiazepines)) in the MOR and KOR systems.....	62
Figure 24 Binding free energy ( $\Delta G_{MM}/PBSA$ ) for each ligand in MOR and KOR systems.....	66

## List of Equations

( 1 ) $V = V_{max}[S]/(S + KM)$ .....	10
( 2 ) $V_{max} = k_{cat}[E]_0$ .....	10
( 3 ) $k_{cat} = V_{max}/[E]_0$ .....	10
( 4 ) $\Delta G_0 = -RT \ln K_{eq} = -RT \ln k_f/k_r$ .....	10
( 5 ) $KM = (k_r + k_{cat})/k_f$ .....	10
( 6 ) $k_r = k_{cat}KM(e^{-\Delta G_0/RT} - 1)$ .....	10
( 7 ) $k_f = k_r e^{-\Delta G_0/RT}$ .....	10
( 8 ) $K_i = [E][I]/[EI] = K_r/K_f$ .....	12
( 9 ) $K_{obs} = K_{inact} \times [I]/(K_{app} + [I])$ .....	12
( 10 ) $CL_{int} = V_{max}/(KM + [S])$ .....	16
( 11 ) $AUC_i/AUC = CL_{int}/CL_{int} - i = 1 + [I]/K_i$ .....	16
( 12 ) $f_b = f_u/B:P$ .....	16
( 13 ) $T_{max} = 1/(K_a - K_{el})/\ln K_a/K_{el}$ .....	22
( 14 ) $t_{1/2} = \ln 2/K_{el}$ .....	22
( 15 ) $Estimated\ CYP = CYP\ Abundance(pmol/mg\ mic\ protein) \cdot$ $MPPGL(mg\ mic\ protein/g\ Liver) \cdot Liver\ Weight(g)/ Liver\ Volume(L)$ .....	22
( 16 ) $AUC\ Ratio = AUC_i/AUC_0$ .....	24
( 17 ) $CL_{int, o} = CL_{int, NOC}/(1 + CH.d/K_i) + CL_{int, OM}$ .....	47
( 18 ) $CL_{int, d} = CL_{int, TMZ} + CL_{int, NDZ}$ .....	47

## PREFACE

I sincerely appreciate my advisor, Dr. Junmei Wang. His instructions and support encourage me a lot to start and finish my project. I learned much from him, not only his expertise and knowledge of study but also his attitude towards study and life. The project he assigned me has highly improved myself.

I would like to express my gratitude the director of our CCGS center, Dr. Xiang-Qun Xie. He gave much support to my work and gave my suggestions for my project.

I would like to thank my committee members, Dr. Junmei Wang, Dr. Xiang-Qun Xie, Dr. Samuel M. Poloyac, Dr. Lirong Wang and Dr. Zhiwei Feng. Their advice enlightened me and helped me better complete my thesis.

I would like to thank Dr. Xibing He and Dr. Viet Man, who help me a lot in my study and life.

I would like to show my gratitude to all the members in our lab and in Dr. Xiang-Qun Xie's group. They all gave me much encouragement when I came with difficulties.

I would like to particularly thank Dr. Samuel M. Poloyac and Dr. Rebecca Price, who helped me and supported me a lot for my projects.

I would like to thank my parents, who gave me support and love.

Lastly, I offer my regards and blessings to all of those who supported me in any aspect during the completion of my projects.

## **1.0 INTRODUCTION**

### **1.1 DRUG ABUSE OF OPIOIDS AND BENZODIAZEPINES**

A key finding in clinical pharmacology and therapeutics is that a majority of overdose fatalities involve multiple drug classes, complicating the drug safety of a specific drug. Combination drug use itself is likely to be a risk factor. For example, sedatives were estimated to be involved in 11,843 deaths in 2014 versus just 1,847 in 1999, whereas sedatives were virtually never the only drug implicated in those deaths [1]. Prescription drug abuse and overdose is a growing problem in the United States. The number of deaths per year due to drug overdose increased 23% in five years, from 38,329 in 2010 to 47,055 in 2014 [2].

Opioids are drugs that can act on opioid receptors and produce morphine-like effects. They have been widely used for pain relief for many years. However, overdose side effects such as nausea, vomiting, coma also exist simultaneously with the benefits of opioids [3, 4]. In the past two decades, the prescriptions of opioid medications have increased tremendously in the United States. There were 16651 deaths related to opioid medications in 2010 [5]. Although overdose deaths are largely assumed as the result of excessive opioid administration alone, the percentage of overdose deaths involving at least one specific drug ranged from 67% in 2010 to 78% in 2014, suggesting opioid abusers are often polydrug abusers [2]. Take heroin as an example, the percentage of poisoning deaths caused by heroin itself increased 42.6% from 2007 to 2014, which was much lower than the percent of change (97.2%) caused by it in combination with other drugs during these 7 years [6].

Benzodiazepines are one of the most commonly co-administered drugs and are often prescribed for patients with anxiety disorders, muscle spasms and major depression [7]. From 2004 to 2011, the rate of nonmedical use-related emergency department (ED) visits for benzodiazepines-opioid co-ingestion increased from 11.0 to 34.2 per 100,000 population, while the prevalence of overdose death involving both drugs increased from 0.6 to 1.7 per 100,000 population [8]. A lot of researchers and physicians have paid attention to the co-administration of these two kinds of drugs since the 1970s [9] Giving that there were approximately 5000 publications related to opioid and benzodiazepines between 1970 and 2012 [9]. Previous studies indicated that although the risks of taking overdose benzodiazepines in isolation are mild, the combination of opioids and benzodiazepines (especially overdose benzodiazepines) posed a potential danger to patients due to the risk of synergistic respiratory depression and overdose death [4, 10-13]. It is believed that opioids and benzodiazepines have complex drug-drug interactions (DDIs), which serve as an important and potentially preventable source of adverse drug effects and overdose death. However, there is still much unknown about how these two types of drugs interact with each other [14].

## **1.2 OXYCODONE**

Oxycodone (OXY), known as Percocet and Oxycontin, is an opioid drug which acts as an agonist of  $\mu$ - and  $\kappa$ -opioid receptors[15]. It is often used as the pain reliever for moderate to severe pain for its effect similar with morphine as well as its high bioavailability (60%) with different formulations, such as oral (most common), intramuscular, intravenous and subcutaneous administration [3]. However, adverse effects of OXY such as constipation, nausea and drowsiness

can be overserved sometimes [16]. OXY was produced from thebaine in 1916 and used in the clinical field in 1917 [17]. The effect of oxycodone is comparable to morphine and it has become one of the most common abuse drugs in recent years.

Oxycodone (6-deoxy-7,8-dehydro-14-hydroxy-3-O-methyl-6-oxymorphine) molecule is a semisynthetic opiate. The bioavailability of OXY is about 62%-87% [18] and it is mostly metabolized with only 10% unchanged in urine. [19] It undergoes cytochromes P450 3A4 (CYP3A4)-mediated N-demethylation to noroxycodone as well as CYP2D6-mediated O-demethylase to oxymorphone, the active metabolite of it. Both noroxycodone and oxymorphone can be further converted to Noroxymorphone [19]. Only a very small amount of oxycodone will undergo conjugation by UDP-glucuronosyltransferases (UGP) [20]. The structure of oxycodone molecule as well as the known metabolic scheme of oxycodone are presented in the Figure 1.

The receptors OXY binds to are opioid receptors which can be found in the central, periphery and autonomous nervous system. Oxycodone can bind to  $\mu$ -,  $\kappa$ - and  $\delta$ -opioid receptors, but it has lower affinity when binding to  $\kappa$ - and  $\delta$ -receptors than  $\mu$ -receptors [21]. These receptors are essentially G protein-coupled receptors (GPCRs), the seven-transmembrane domain receptors, which can activate intracellular activities when coupling with G proteins [16].

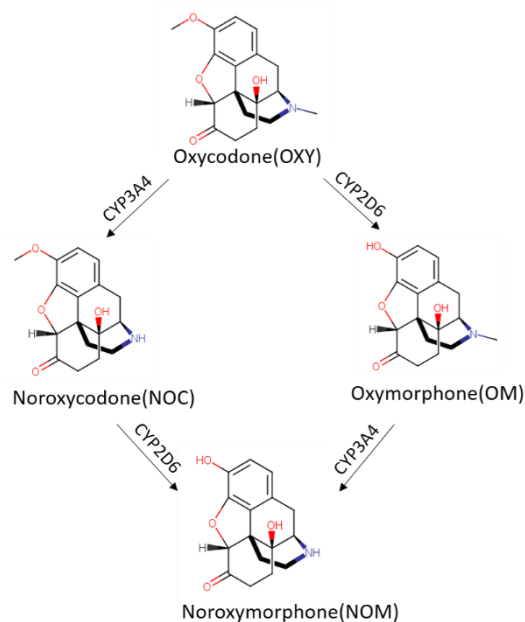


**Figure 1 The metabolic path ways of oxycodone.**

### 1.3 DIAZEPAM

Diazepam (DZP) is a long-acting benzodiazepine with its brand name Valium. It is one of the most frequently prescribed benzodiazepines and is widely accepted and used by people for the treatment of anxiety, muscle spasms, seizures, trouble sleeping, etc. [22]. DZP has a calming effect and it can be administered by mouth, rectum injection, muscle injection and vein injection. The overdose effects of taking DZP alone are drowsiness, mental confusion and coma. Concurrent use of diazepam and other drugs like alcohol and opiates may be fatal [23].

DZP is a classical long-acting aryl 1, 4-benzodiazepine with no hydrogen bond donors [22]. It is mainly metabolized in the liver by cytochrome P450-mediated reactions (Figure 2). DZP undergoes CYP3A4 and CYP2C19-mediated bioactivation to yield nordazepam (NDZ) (N-

demethylation) and temazepam (TMZ) (3-hydroxylation), respectively. Both metabolites can be further converted to oxazepam (OZP) [24]. It can also be metabolized by CYP2C18 and CYP2C9 though with relatively low  $K_m$ . Generally, CYP2C19 contributes major to the N-demethylation while CYP3A4 makes the main contribution to the 3-hydroxylation. The bioavailability of DZP is more than 90% and its plasma protein binding fraction is also very high (approximately 97%), which leads to its long half-life ( $43 \pm 13$  hours) [25].

DZP is also the positive allosteric modulator of the GABA type A receptor ( $GABA_A$ ) which mediates most of the pharmacological effects of DZP [22].  $GABA_A$  is a transmembrane hetero-oligomeric protein mainly found in the central nervous system (CNS) and peripheral area [26]. It belongs to a gene superfamily of ligand-gated ion channels and is activated by  $\gamma$ -aminobutyric acid (GABA), the primary inhibitory neurotransmitter in the central nervous system [26, 27].

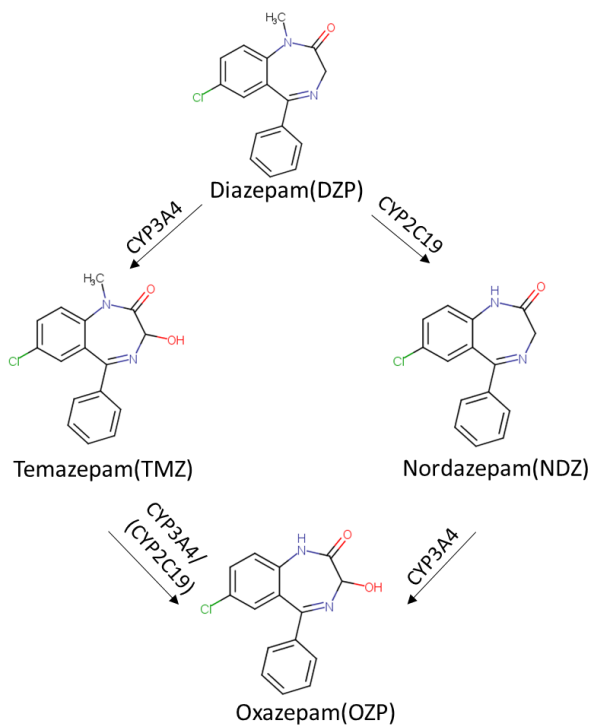


**Figure 2 The metabolic pathways of diazepam.**

## 1.4 DDI MECHANISM

It is believed that opioids and benzodiazepines have complex drug-drug interactions (DDIs), which serve as an important and potentially preventable source of adverse drug effects and overdose deaths. However, there is still much unknown about how these two types of drugs interact with each other [14].

Since DDIs can be broadly categorized as pharmacokinetics (PK) or pharmacodynamics (PD), one possible mechanism to explain the interaction is that benzodiazepines may alter the pharmacokinetic properties of opioids. Pharmacokinetic DDIs may occur when a co-administrated drug causes a change in the absorption, distribution, metabolism, and/or excretion (ADME) of another drug [28]. Opioids undergo phase I metabolism through CYP3A4 enzyme, and therefore, may have significant interactions with other co-administrated drugs that are CYP3A4 substrates, inhibitors, or inducers [29]. Some benzodiazepines have been reported as CYP3A4 inhibitors since they are also mainly metabolized by the CYP3A4 system [30-35]. Since CYP3A4 is the common major player in metabolism pathways of both oxycodone (OXY) and diazepam (DZP), we wonder if DZP can affect OXY's activity of metabolism.

Some studies suggested that co-administration of benzodiazepines with opioids can potentially increase opioid exposure. Research utilizing human liver microsomes demonstrated that midazolam is a moderate mechanism-based inactivator of buprenorphine N-dealkylation, which can cause time- and concentration-dependent inhibition of norbuprenorphine formation (metabolized in part by CYP3A4) [36]. By quantitatively analyzing the plasma concentration of oxycodone and clonazepam, a case report also indicated that concomitant clonazepam intake can reduce oxycodone's metabolism [37].

Another mechanism that underlies the interaction between these two drugs is pharmacodynamics. Some preclinical evidence shows some effects of benzodiazepines like analgesic and anxiolytic are partially mediated by opioidergic mechanisms, but there are also some studies reported contrasting data in terms of the evidence [9]. However, it is believed that people may concomitantly take opioids and benzodiazepines to increase the  $\mu$  agonist effects of opioids. It is reported that 72 % of patients who use methadone are also diazepam users simultaneously, indicating that diazepam can enhance the drug effects of methadone [38].

Because the DDI studies of the two types of drugs in human subjects are limited, alternative methods for evaluating DDIs at toxic levels in humans are needed. To the best of our knowledge, the physiologically based pharmacokinetic (PBPK) modeling of the DDI between oxycodone and diazepam has not been reported. In this work, we aimed to first quantitatively simulate the PK profiles of oxycodone and diazepam by utilizing both the experimental PK and (PBPK) modeling, then use molecular modeling techniques such as molecular docking, molecular dynamics simulation and binding free energy calculations using MM/PBSA (Molecular Mechanics/Poisson Boltzmann Surface Area) to predict the pharmacodynamic interaction between these two drugs. The extent of DDIs between the two drugs due to PK or pharmacological interaction can be estimated from those simulations.

## **2.0 METHODS**

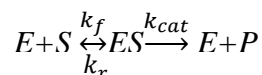
### **2.1 PHARMACOKINETICS**

For pharmacokinetic DDI study, we first used the simplest experimental model to generally investigate the possible DDI between oxycodone (OXY) and diazepam (DZP) in their metabolic pathways. Secondly, a full physiologically-based pharmacokinetics (PBPK) model was selected to predict their interaction in a complicated whole human body by using the software Simcyp. The PBPK-based DDI simulations were conducted with a virtual healthy population of 100 subjects and using the default systems data for the population implemented in Simcyp. The interaction profiles of other opioids (fentanyl and buprenorphine) and benzodiazepines (midazolam, alprazolam and triazolam) were also simulated. Drug data come from literature and were predicted by Simcyp if not available. Finally, we selected a less complex minimal PBPK model utilizing the Matlab-Simbiology software to predict the pharmacokinetic DDI between OXY and DZP again to see if the minimal PBPK model can achieve similar results as the full PBPK model does.

#### **2.1.1 Empirical PK modeling**

A simple empirical pharmacokinetics (PK) model was constructed to simulate the interactions between OXY and DZP. The homogeneous one compartment model concomitantly includes both liver and plasma (Figure 3). Although simple, the model allows us to quickly learn about the pharmacokinetic DDIs between the two drugs.

PySB [39] is a framework for quantitatively building models of biochemical systems in a Python environment. PySB was primarily developed by the Sorger Lab at Harvard Medical School and the Lopez Lab at Vanderbilt University. It is mainly applied to express processes of interactions among multiple proteins and/or other bio-actives through enzymatic reactions with a simple and intuitive domain specific programming language based on Python. For example, PySB can be used to simulate a typical enzyme-catalyzed reaction as given below.



Where  $k_f$  is the forward reaction rate constant of  $E+S$ ,  $k_r$  is the reverse reaction constant describing rate of falling apart to  $E+S$  from  $ES$  (enzyme-substrate complex) and  $k_{cat}$  is the forward rate constant of the formation of  $E+P$ . Provided  $k_f$ ,  $k_r$ ,  $k_{cat}$  in each metabolic pathway of OXY and DZP, as well as the amount of drugs and enzymes, we can simulate the complex process of reactions when both OXY and DZP are involved.

It is common that pharmacokinetic parameters are missing and must be estimated in PK modeling. We performed molecular modeling studies to calculate binding affinities between a drug molecule and its cytochrome P450 targets using docking simulations. We used the docking affinities together with the Michaelis-Menten constant,  $k_m$  to calculate forward and reverse reaction constants. All the docking simulations were performed using the Glide module [40, 41] implemented in Schrodinger's small-molecule drug discovery suite ([www.schrodinger.com](http://www.schrodinger.com)). The canonical docking protocol was followed to prepare the receptor structure and the grid files [42]. Flexible docking simulations using the standard precision docking scoring functions were performed for the OXY and DZP binding to CYP3A4, CYP2D6 and CYP2C19, the three major

cytochrome P450 enzymes metabolizing the two drugs. With the calculated binding affinities,  $k_f$  and  $k_r$  parameters can be calculated using Equations 1-7 [43-45].

$$(1) V = V_{max} \frac{[S]}{[S] + K_M}$$

$$(2) V_{max} = k_{cat} [E]_0$$

$$(3) k_{cat} = \frac{V_{max}}{[E]_0}$$

$$(4) \Delta G^0 = -RT \ln K_{eq} = -RT \ln \frac{k_f}{k_r}$$

$$(5) K_M = \frac{k_r + k_{cat}}{k_f}$$

$$(6) k_r = \frac{k_{cat}}{K_M e^{\frac{\Delta G^0}{RT} - 1}}$$

$$(7) k_f = k_r e^{-\frac{\Delta G^0}{RT}}$$

Where Equation 1 is the Michaelis-Menten equation and  $K_M$  is the substrate concentration at which the reaction rate  $V$  is the half of maximum reaction rate  $V_{max}$ .  $[S]$  is the substrate concentration and  $[E]_0$  is the total concentration of enzyme ( $[E] + [ES]$ ).  $K_{cat}$  can be calculated with Equation 3.  $\Delta G^0$  is the binding free energy which can be estimated using the Glide docking score (kcal/mol).  $K_{eq} = K_f/K_r$ , is the equilibrium constant for a reversible reaction.  $K_f$ ,  $k_r$  can be calculated by Equations 6 and 7.

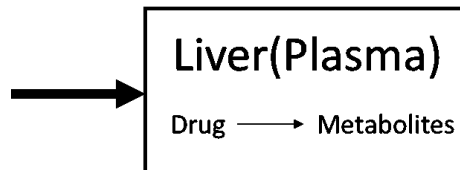


**Figure 3 Empirical PK model.**

### 2.1.2 Full PK modeling

Physiologically based pharmacokinetic (PBPK) modeling has been increasingly used for the prediction of drug-drug interaction (DDI) recently, especially for the prediction of CYP-mediated DDIs [46]. This modeling utilizes in vitro drug data (e.g. intrinsic clearance and bioavailability) through the description of absorption, distribution, metabolism and elimination (ADME) and system data which depicts physiological properties of human subjects in a population to explore in vivo pharmacokinetics of drugs and DDI scenarios. The PBPK approach has been valued by the US Food and Drug Administration (FDA) and European Medicines Agency (EMA) through the guidelines for DDIs in 2012 and 2013 [47]. PBPK modeling currently receives high attention in the drug development and drug discovery process. A PBPK model consists of multiple compartments which represent different physiological organs of the human body. Circulating blood system links all of the compartments. Similar full PBPK models are built for both oxycodone and diazepam, the only difference between the models of these two drugs is the absorption process. We assume oxycodone undergoes the first-order absorption while Advanced Dissolution, Absorption and Metabolism (ADAM) model is applied for diazepam absorption process. ADAM model considers the complicated process of drug absorption and interplays with the underlying physiological characteristics of the gastrointestinal (GI) tract [48, 49]. The generic full PBPK model and ADAM model are shown in Figure 4.

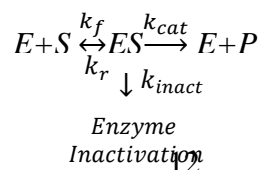
The Simcyp Simulator (Version 17 Release 1, Sheffield, UK) was used in the development of full PBPK modeling. It is the simulator for population-based PK modeling by linking in vitro data to in vivo ADME and PK/PD outcomes, which can help industries design dose strategy and inform product labeling. We chose the healthy volunteer population in the Simcyp database to

predict the PK profiles of drugs. All of the PK parameters for the two types of drugs are summarized in the APPENDIX (Table S1). Particularly, because there is no exact experimental data for  $K_i$  value of oxycodone and diazepam, we did Glide docking and chose the best poses which not only have similar binding modes as the co-crystallized ligand of CYP3A4, but also have relatively high docking scores. Then we calculated the  $K_i$  values for these two drugs (especially for diazepam) using the docking score by Equation 8. The  $K_i$  values were utilized in competitive inhibition. The docking poses for oxycodone and diazepam are shown in Figure 5 and the docking scores and calculated  $K_i$  are listed in Table 1. To explore how significant of  $K_i$  parameters influence the PBPK simulation results, the sensitivity analysis was also conducted to investigate the impact of  $K_i$  values towards the DDI effect, utilizing the Simcyp built-in sensitivity analysis function.

$$(8) K_i = \frac{[E][I]}{[EI]} = \frac{K_r}{K_f}$$

Besides competitive inhibition, mixed type inhibition which includes both competitive and mechanism-based inhibitions are applied to predict the DDIs between two drugs. Mechanism-based inhibition occurs when a drug's binding to CYP enzyme is fully or partially irreversible (such as forming covalent bonds), which lead to the inactivity of CYP enzyme and changes of PK parameters, such as  $K_i$  (half-maximal inactivation) and  $k_{inact}$  (inactivation rate of enzyme) [50]. The  $k_{inact}$  and  $k_{app}$  were evaluated by fitting and extrapolation Equation 9 which describe the relationship between the observed inactivation rate constants ( $k_{obs}$ ) and the concentration of the test inhibitor ([I]). The schematic diagram of mechanism-based inhibition was exhibited below.

$$(9) K_{obs} = \frac{K_{inact} \times [I]}{K_{app} + [I]}$$



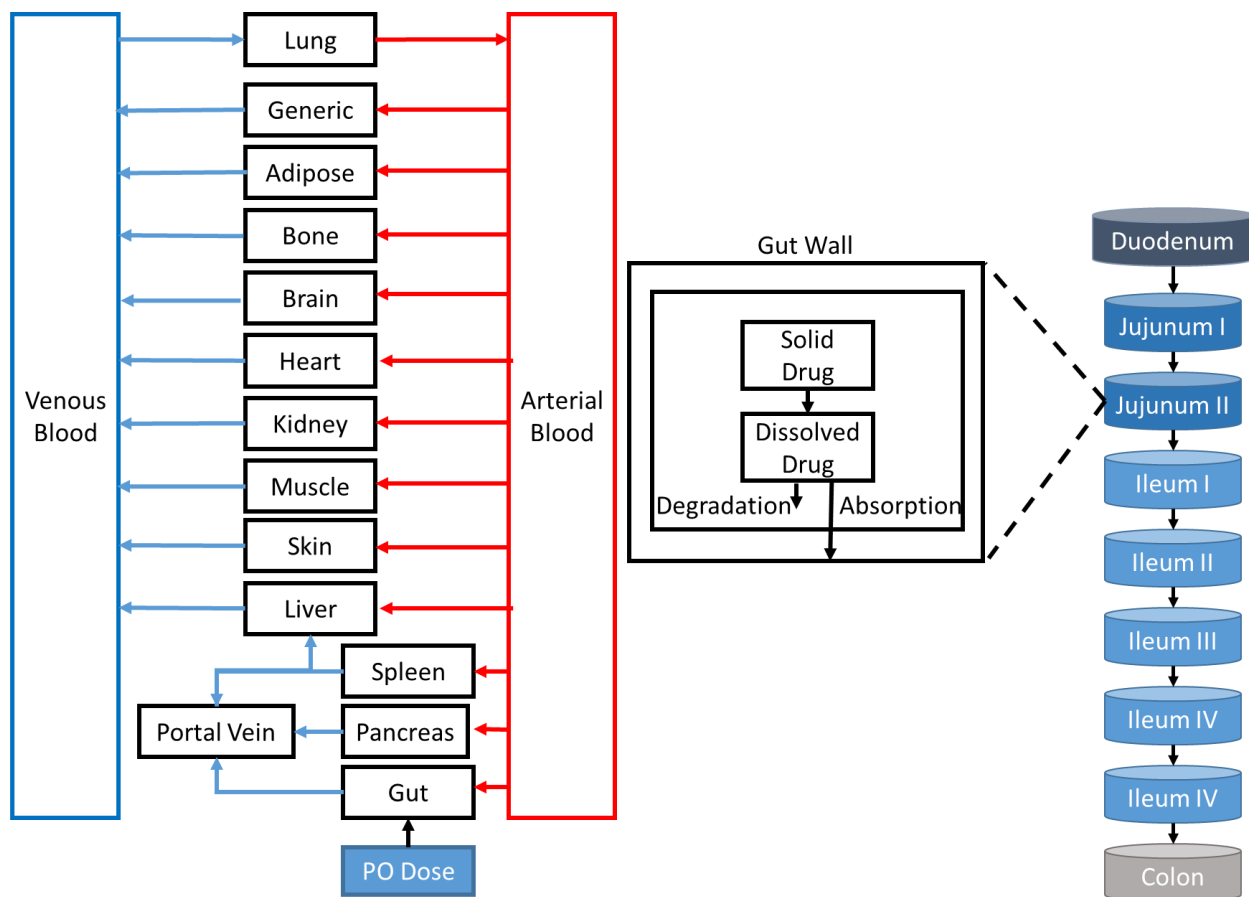


**Figure 4** The PBPK model (left panel) and ADAM model (right panel).

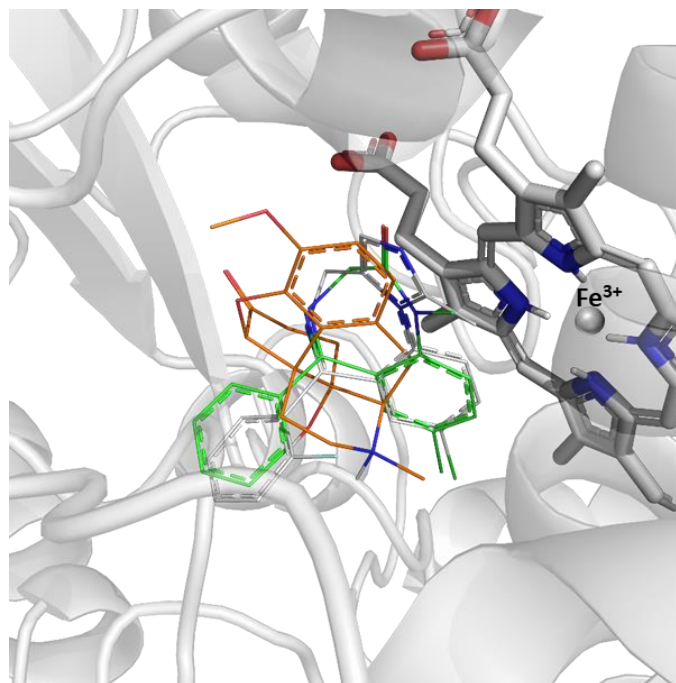


**Figure 5 The docking poses of oxycodone and diazepam in CYP3A4.**

The orange ligand is oxycodone, the green ligand is diazepam, the white ligand which partially overlapped with oxycodone and diazepam is the co-crystallized ligand of CYP3A4. The heme group, a coordination complex consisting of an iron ion in cytochrome P450, is shown as sticks.

**Table 1 The docking scores and calculated  $K_i$  for oxycodone and diazepam CYP3A4.**

	Docking Score (kcal/mol)	Calculated $K_i$ ( $\mu$ M)
oxycodone	-6.77	10.9
diazepam	-7.89	1.65

### 2.1.3 Minimal PK modeling

Physiologically-based pharmacokinetic models were developed respectively for oxycodone (OXY) and diazepam (DZP) to predict their pharmacokinetic interaction *in vivo* using

the parameters either from literature or estimated values by fitting *in vitro* data. Minimal PBPK models were chosen because OXY and DZP are both predominately metabolized in liver. Only less than 1% of DZP is excreted by kidney, while up to 19% of OXY is excreted after an oral dose by kidney [25]. The major difference of minimal PBPK models from a complete PBPK model lies in that organs and tissues are modeled separately in the latter, while the former assumes that the plasma compartment contains tissues that have similar drug distributions except for the hepatic compartment [51, 52]. Applying a minimal PBPK model can minimize the inaccuracy caused by lack of parameters for other less important organs and systems. For OXY and DZP, our minimal PBPK model only keeps the essential parts of a complete PBPK model, including liver, blood flow as well as drug partitioning among the applied compartments. The model for each drug is composed of systemic blood, hypothetical portal vein and liver compartments as shown in Figure 6.

Simbiology® is a systems biology toolbox implemented in Matlab (R2017b). It is a popular platform to model, simulate and analyze the systems biology data with an extra focus on PK/PD modeling and simulation. It was selected to create a semi-PBPK model because of its versatile model exploration techniques and strength to simulate the time course profiles of drug exposure based on various ordinary differential equations (ODEs) or stochastic solvers.

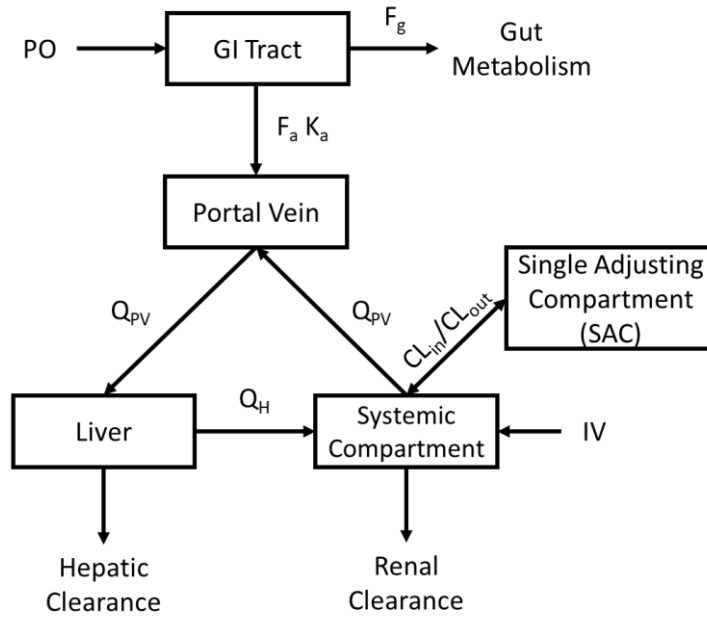


**Figure 6 The minimal PBPK model.**

$Q_{pv}$  is the blood flow rate from systemic blood to portal vein or from portal vein to liver;  $Q_H$  is the blood flow rate from liver to systemic blood;  $F_a$  is fraction absorbed from the gastrointestinal tract;  $F_g$  is gut availability (fraction of drug escaping from the gut availability);  $K_a$  is the absorption rate;  $CL_{in}/CL_{out}$  is the clearance into and out of the single adjusting compartment.

Metabolisms of OXY, DZP as well as their metabolites were considered in the minimal PBPK model to study the pharmacokinetic interaction between two drugs. Hepatic intrinsic clearance ( $CL_{int}$ ) is the parameter which describes the intrinsic ability of the liver to remove (metabolize) the drug. It is defined by Equation 10.

$$(10) CL_{int} = \frac{V_{max}}{K_M + [S]}$$

$$(11) \frac{AUC_i}{AUC} = \frac{CL_{int}}{CL_{int-i}} = 1 + \frac{[I]}{K_i}$$

$$(12) f_b = \frac{f_u}{B:P}$$

If there is an inhibitor which acts on the same enzyme of substrate via the competitive inhibition mechanism, the relationship between  $AUC_i/AUC$ ,  $CL_{int-i}/CL_{int}$  and  $K_i$  can be described by Equation 11. Where  $[I]$  is the concentration of an inhibitor with the inhibitory constant of  $K_i$ ,  $f_{b,o}$  and  $f_{b,d}$ , which are defined in Equation 12, represent the unbound fractions of OXY and DZP in blood, correspondingly.  $f_u$  is the unbound fraction of drug in plasma and B:P represents the blood and plasma concentration ratio.  $K_p$  is the liver-to-blood concentration ratio of a drug (assumed to be 1 for all drugs in this study) [44].  $K_i$  is the inhibitory constants of DZP which is estimated using its binding affinity to CYP3A4 with Equation 8. All the PK parameters used are also listed in APPENDIX (Table S2).

## 2.2 PHARMACOKINETICS

For pharmacodynamics (PD) DDI study, we decided to investigate the binding situation of benzodiazepine with  $\mu$ - and  $\kappa$ -opioid receptors by utilizing molecular modeling techniques, since oxycodone is an agonist of  $\mu$ - and  $\kappa$ -opioid receptors. We plan to find out if benzodiazepines can also have positive effects on the two opioid receptors. Agonist-bound and antagonist-bound  $\mu$ - and  $\kappa$ -opioid receptors were downloaded from Protein Data Bank (<http://www.rcsb.org>); opioids and benzodiazepines were downloaded from PubChem (<https://pubchem.ncbi.nlm.nih.gov/>). Molecular docking, molecular dynamics simulation and MM/PBSA calculations were performed step by step as detailed below.

### 2.2.1 Molecular docking

Molecular docking was performed using the Glide module of the Schrodinger suite of software (Maestro, version 11.2) for the aforementioned receptors: active  $\mu$ -opioid receptors (PDB Code 5C1M, co-crystallized agonist 4VO), inactive  $\mu$ -opioid receptor (PDB Code 6B73, co-crystallized antagonist CVV), active  $\kappa$ -opioid receptor (PDB Code 4DJH, co-crystallized agonist JDC), and active  $\kappa$ -opioid receptor (PDB Code 4DKL, co-crystallized antagonist BF0). For each receptor, the “Protein Preparation Wizard” was first applied to prepare the receptor structure for the Glide docking including adding hydrogens, creating disulfide bonds, conducting restraint minimization, etc. Glide grid was then generated with default setting. For example, the van der Waals radius scaling factor is 1.0 and partial charge cutoff is 0.25. The grid site was automatically set to the central location of workspace ligand and its size was manually adjusted to match the size of co-crystallized ligand without any constraints or rotatable groups. In total, twelve ligands were selected for the docking studies: four co-crystallized ligands of  $\mu$ - and  $\kappa$ -opioid receptors (4VO, CVV, JDC, BF0), four opioids (oxycodone, methadone, buprenorphine, naltrexone) and four benzodiazepines (alprazolam, diazepam, midazolam, triazolam). Flexible ligand docking was then performed with the default setting (the van der Waals radius scaling factor is 0.80, partial charge cutoff is 0.15 for ligands, no constraints, etc.) except that the “reward intramolecular hydrogen bonds” was turned on and the maximal poses per ligand was set to 10. In most situations, the best docking poses ranked by the Glide “Standard Precision” docking scoring function were selected for the subsequent modeling studies. Sometimes, other top docking poses were selected if they can much better overlap with the co-crystallized ligands.

### 2.2.2 Molecular dynamics simulations

The starting conformations of the membrane for the opioid receptor complex were built using CHARMM-GUI [53] after making the longest principal of axis along to the Z-axis and the coordinate center of 7TM is in origin. 240 POPC lipid molecules were added. The complexes were immersed in a rectangle box with TIP3P water molecules [54] in all three dimensions. A set of  $\text{Na}^+$  and  $\text{Cl}^-$  ions were added to make a 0.15 M concentration of NaCl and to neutralize the whole systems.

In molecular mechanics (MM) minimizations and MD simulations, the parameters for ligands and atom types were carried out by the General Amber force field (GAFF) in AMBER 16 [55]. The atomic partial charges were derived by restrained electrostatic potential (RESP) [56] to fit the HF/6-31G\* electrostatic potentials generated using the Gaussian 16 software package [57]. All topologies in MD were generated using the Antechamber module [58].

MD simulations were performed using the PMEMD.mpi and PMEMD.cuda modules in the AMBER 16 package [59-61]. At first, to remove possible steric crashes in the systems, five steps of energy minimization were employed. Water and ions were relaxed first, followed by the protein and ligand complex. The harmonic restraint force constants reduced step by step from 20 to 10, 5, 1 and finally to 0 kcal/mol/Å<sup>2</sup>. After the minimization, the temperature of each system was heated from 0 to 300 K and was kept at 300 K. The pressure was controlled at 1atm with the relaxation time of 2 ps. The temperature was regulated by Langevin dynamics [62, 63]. To constrain all hydrogen atoms, the SHAKE algorithm [64] was applied and the time was set to 0.001 ps. After a 20 ns equilibration, the MD trajectory was collected for 200 ns and each snapshot was saved every 100 ps.

### 2.2.3 MM/PBSA calculations

The Molecular Mechanics/Poisson-Boltzmann Surface Area (MM/PBSA) approach [65] is based on MD simulation and has been commonly used in the prediction of binding free energies. It can decompose the binding free energy into different interaction terms and each energy component is computed from series of conformational snapshots taken from MD simulations [66].

In MM/PBSA, the binding free energy ( $\Delta G_{MM/PBSA}$ ) between a ligand and a receptor to form a complex is calculated as the equations below.

$$\Delta G_{MM/PBSA} = \Delta H - T\Delta S = \Delta E_{inter} + \Delta E_{ele} + \Delta E_{vdw} + \Delta G_p^{sol} + \Delta G_{np}^{sol} - T\Delta S$$

$\Delta E_{inter}$  is the change of internal bonded MM energy,  $\Delta E_{ele}$  is the change of MM electrostatic energy,  $\Delta E_{vdw}$  is the change of MM van der Waals energy,  $\Delta G_p^{sol}$  is the polar solvation free energy,  $\Delta G_{np}^{sol}$  is the nonpolar solvation free energy, T is the absolute temperature and  $\Delta S$  is the change of entropy.

Because in the real application, it is more common to simulate only complex state, causing the removal of  $\Delta E_{ele}$ . So the equation is changed to:

$$\Delta G_{MM/PBSA} = \Delta H - T\Delta S = \Delta E_{vdw} + \Delta G_p^{sol} + \Delta G_{np}^{sol} - T\Delta S$$

For each MD snapshot, the binding free energy of each ligand was calculated and the detailed free energy compositions were performed for all snapshots in the sampling phases of MD simulations. The Poisson Boltzmann calculations were performed with the Delphi program [67].

## **3.0 RESULTS**

### **3.1 PHARMACOKINETICS**

Empirical PK model, full PBPK model and minimal PBPK model were first created and individual PK profiles for opioids and benzodiazepines were then generated. We collected experimental data of PK profiles for these two kinds of drugs from literature and used it to verify our models. Last the profiles of DDI between the two types of drugs were generated using PySB, Simcyp and Simbiology software. In all the (PB)PK models, opioids served as substrates while benzodiazepines as inhibitors. AUC (Area under the curve) were compared between substrate and substrate-inhibitor profiles to investigate the DDI between these two kinds of drugs.

#### **3.1.1 Empirical PK modeling**

The application of molecular modeling techniques, such as docking simulations, to facilitate the acquisition of PK parameters is credible and can be explored to expand the applications in the future. By applying the PK parameters from docking to PySB, the concentration-time (C-T) profiles can be generated. The simulation results showed DZP only has a weak inhibitory effect on the CYP3A4 enzyme for OXY, even though DZP is a stronger binder to CYP3A4 than OXY. The PySB scripts for the empirical PK model were shown in the APPENDIX CODE.

We assumed that OXY and DZP are administered orally and the oral dosage of OXY is 40mg (127  $\mu\text{mol}$ ) [15, 17] while the dosage of DZP is 10mg (31.5  $\mu\text{mol}$ ) [68, 69]. When the drug absorption and elimination follow the first-order reaction, the absorption rate and elimination rate constants ( $K_a$ ) can be estimated with Equations 13-14 [70].

$$(13) T_{max} = \left( \frac{1}{K_a - K_{el}} \right) \ln \frac{K_a}{K_{el}}$$

$$(14) t_{1/2} = \frac{\ln 2}{K_{el}}$$

Where  $T_{max}$  is peak time, and  $K_{el}$  is the elimination rate constant. The average time to achieve peak plasma concentration for DZP is 1.3 hours [25] while the half time  $t_{1/2}$  is 43 hours [25]. Combining Equations 6 and 7, the  $K_a$  of DZP ( $K_{a,d}$ ) was estimated to be 4  $\text{hr}^{-1}$  (0.0011  $\text{s}^{-1}$ ). The  $K_a$  of OXY ( $K_{a,o}$ ) is set to be 0.7  $\text{hr}^{-1}$  according to literature [71].

The metabolism of OXY is involved with enzymes CYP3A4 and CYP2D6. CYP3A4 and CYP2C19 are the enzymes participated in the metabolic pathways of DZP. The liver is assumed to be homogeneous tissue and the total concentration of each enzyme is estimated with Equation 15.

$$(15) \text{Estimated } [CYP] = \frac{\text{CYP Abundance} \left( \frac{\text{pmol}}{\text{mg mic protein}} \right) \cdot \text{MPPGL} \left( \frac{\text{mg mic protein}}{\text{g Liver}} \right) \cdot \text{Liver Weight}(\text{g})}{\text{Liver Volume}(\text{L})}$$

[CYP] here is the concentration of cytochrome P450 in liver. MPPGL, the microsomal protein per gram of human liver, is set to 45  $\text{mg} \cdot \text{g}^{-1}$  liver. The average liver weight is around 1.5 kg [72] and liver volume is estimated to be around 1.5 L [73]. The abundance of CYP3A4, CYP2D6 and CYP2C19 is therefore estimated to be 137  $\text{pmol} \cdot \text{mg}^{-1}$  (of microsomal protein), 8  $\text{pmol} \cdot \text{mg}^{-1}$  and 14  $\text{pmol} \cdot \text{mg}^{-1}$ , respectively. Those values can be transformed to 6.165  $\mu\text{M}$ , 0.36  $\mu\text{M}$  and 0.63  $\mu\text{M}$  in the liver.

The  $K_M$  and  $V_{max}$  of each pathway were derived from literature and are shown in Table 2. OXY, DZP and their metabolites were docked to the three cytochrome P450 enzymes. The best docking scores were listed in Table 2. The best docking scores for OXY and DZP bind to CYP3A4 were shown in Figure 5. The rest binding poses were shown as the supplementary materials (Figure S1 and Figure S2).  $k_f$ ,  $k_r$  and  $k_{cat}$  listed in Table 2 were derived according to Equations 1-7. The value of  $K_M$  and  $V_{max}$  for OXY and DZP were obtained from literature [19, 24, 74, 75].

The concentrations of drugs have been transformed to describe the corresponding concentrations in plasma, though the concentration variation was closer to the real reaction rate in liver. Figure 7 depicted the concentration of 40 mg single dose OXY before and after co-administrated with different sizes of single dose DZP. While the dose of OXY was always 40 mg, the dose of DZP increased from 10 mg, 20 mg, 50 mg to 100 mg (Groups A, B, C, D, accordingly). When the dosage of DZP was 100 mg, the maximal concentration of diazepam was 2250 ng/mL. According to a report, even when plasma concentration of the diazepam was as high as 4792 ng/mL, patients were minimally sedated and were discharged within 24 h [76]. The concentration ~ time (C-T) curve for OXY administered by itself is shown as the red dashed line, while the C-T curves for OXY administered concomitantly with different doses of DZP are shown in blue-solid lines. The concentration of OXY became a little bit higher when the two drugs were given simultaneously and increasing the dose of DZP amplified the trend. The AUC (area under the concentration-time curve) ratio was calculated with Equation 16 and was listed in Table 3, where  $AUC_i$  is the AUC with an inhibitor present and  $AUC_0$  is the AUC without the participation of an inhibitor. The AUC ratio is almost the same for Groups A and B, with the difference being only 0.01. The AUC ratio of Group C is 3.96% higher than that of Group A. When the dose amount of

DZP is 10 times larger than the regular dose, the  $AUC_R$  increases to 9.9% compared to that of Group A.

$$(16) AUC \text{ Ratio} = \frac{AUC_i}{AUC_0}$$

**Table 2 Parameters used in empirical PK modeling.**

	Docking score	$K_M(\mu\text{M})$	$V_{\max}(\mu\text{mol}\cdot\text{s}^{-1})$	$k_{\text{cat}}(\text{s}^{-1})$	$k_f$ ( $\mu\text{M}^{-1}\cdot\text{s}^{-1}$ )	$k_r(\text{s}^{-1})$
OXY-NOC(3A4)	-6.77	377	0.7245	0.0783	0.000218	0.0039
OXY-OM(2D6)	-6.43	39.8	0.1026	0.19	0.00928	0.179
NOC-NOM(2D6)	-7.375	20.5	0.1341	0.248	0.014956	0.0586
DZP-TMZ(3A4)	-7.89	140	4.6245	0.5	0.003619	0.00661
DZP-NDZ(3A4)	-7.89	152	0.4155	0.045	0.0003	0.000547
DZP-NDZ(2C19)	-7.083	21	0.02775	0.0293	0.00201	0.0129
TMZ-OZP(3A4)	-7.794	307	0.204	0.022	0.000072	0.000139
NDZ-OZP(3A4)	-7.364	94	0.573	0.062	0.000689	0.00275

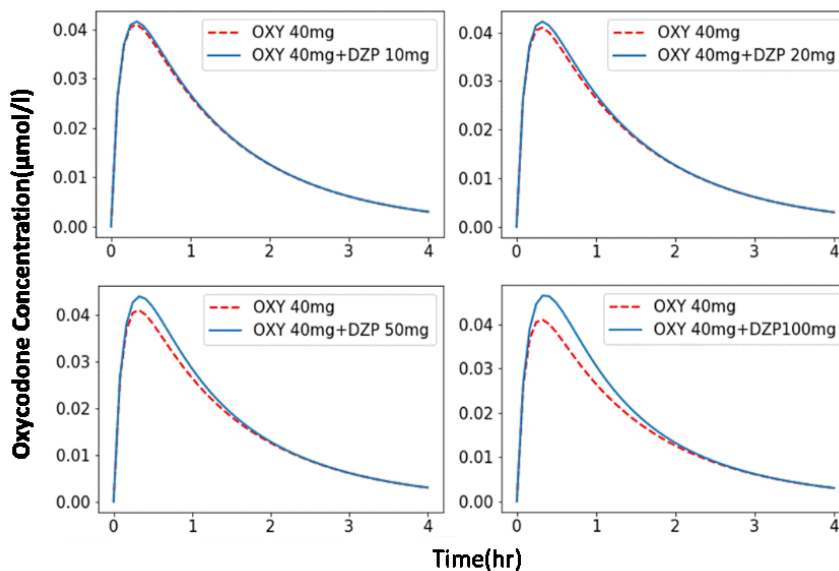


**Figure 7** The Concentration-Time curves of 40 mg OXY co-administered with 10 mg, 20 mg, 50 mg, and 100 mg DZP from PySB.

**Table 3** AUC ratios when using OXY and different dose of DZP together in PySB.

Group	Dosages	AUC Ratio
A	OXY 40mg+DZP 10mg	1.01
B	OXY 40mg+DZP 20mg	1.02
C	OXY 40mg+DZP 50mg	1.05
D	OXY 40mg+DZP 100mg	1.11

**Discussion** A one-compartment empirical model highlights the metabolic interaction between OXY and DZP and is a convenient way to find whether DZP can alter PK profile of OXY. To validate our computational protocol of applying molecular docking to estimate reaction rates, we created the same PK model in Simbiology with  $k_f$ ,  $k_r$ ,  $k_{cat}$  being replaced with  $K_M$  and  $V_{max}$  parameters. The C-T profiles for oral administration of 40 mg OXY predicted by the two software

are shown in Figure 8. The AUC by using  $k_f$ ,  $k_r$ , and  $k_{cat}$  to express metabolic processes in PySB was  $0.065 \mu\text{mol}\cdot\text{hr}\cdot\text{l}^{-1}$ , which was almost identical to  $0.0638 \mu\text{mol}\cdot\text{hr}\cdot\text{l}^{-1}$ , the AUC acquired by inputting  $K_M$  and  $V_{max}$  to simulate the same metabolism in Simbiology. Therefore, applying molecular modeling is a promising way to obtain high quality PK parameters for mechanistic PK modeling. It is also noted that this methodology is not restricted to the metabolic process but can also be used for the target binding, which implies a possibility to build a bridge between pharmacology and PK mathematical processes.

Although the simulated C-T profiles are for OXY and DZP in plasma, they reflect the kinetics and metabolism of the two drugs in the liver, making it easier to find the metabolic influence of DZP on OXY. Since CYP3A4 is a major enzyme involved in the metabolic pathways of both OXY and DZP, the change on the C-T profile of OXY upon the co-administration of DZP can be applied to measure the pharmacokinetic DDI between the two drugs. If the competitive binding of DZP to CYP3A4 causes a reduction of free CYP3A4 enzyme, the catalysis of OXY may be slowed, leading to the accumulation of OXY in the human body. However, the simulation results suggested that the PK interaction between OXY and DZP was very small and the  $\text{AUC}_R$  only grew 0.01 for the normal dosage (Table 2 and Table 4). This finding is consistent with the statement that benzodiazepines might be weak competitive inhibitors to CYP3A4 [4, 77]. It is also found that increasing doses of DZP (from 10 mg to 20 mg, 50 mg and 100 mg) can increase the inhibitory effect of DZP as the  $\text{AUC}_R$  increased proportionally (from 1.01, 1.02, 1.05 to 1.11). This suggests that higher doses of DZP can cause the overdose effect of OXY. A study investigating the association between benzodiazepine prescribing patterns and the risk of death from opioid analgesics overdoses among US veterans [78] found that the unadjusted rates of death from an overdose of OXY increased in combination with higher daily benzodiazepine doses. However,

according to our simulation results, even when the dosage of DZP highly rises (rising over 10 times), pharmacokinetic DDI can be hardly observed between the two drugs, implying there is limited PK interaction between these two drugs, side effects caused by combination of two drugs are more likely due to PD interaction between them. The limitation for this model is the predicted concentration for the drug is lower than real situation. For example, the maximal concentration of oxycodone predicted by this model is around 0.04  $\mu\text{M/L}$  (12.6 ng/mL), which is lower than the usual maximal concentration of the same dosage of oxycodone [79]. This can be explained by this particular homogeneous model which only has one single compartment and everything is included in it, thus the simulated concentration of the drug would be underestimated because it is assumed to be averagely distributed in the body.

The PK modeling is becoming an essential part of drug discovery, but it is very challenging to build predictive models since many PK parameters are not available. Our novel methodology of utilizing molecular modeling to assign parameters for PK modeling can be a breakthrough because it offers a reliable and practical way to investigate DDIs for drugs that lack experimental PK data, which can inspire investigators to study DDIs even when the experimental data is unavailable. Furthermore, this technology is not only restricted to the metabolic process but can also be used for target binding, expanding the investigation of PD interactions, which implies a possibility to build a bridge between pharmacology and PK mathematical process.

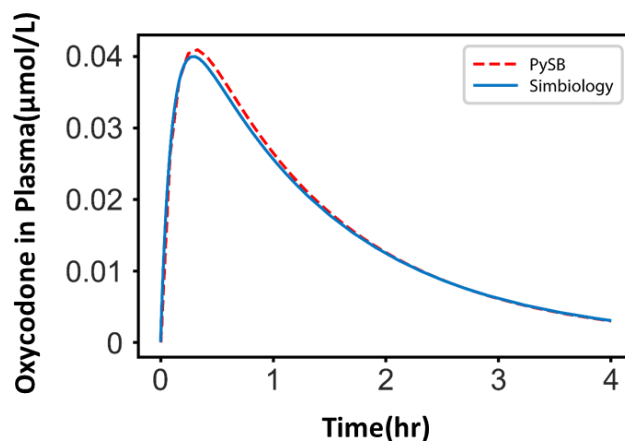


**Figure 8 The concentration of OXY in empirical PK model predicted by PySB and Simbiology.**

### 3.1.2 Full PK modeling

The PK parameters of ADME processes for oxycodone (OXY) and diazepam (DZP) as well as their metabolites were listed in APPENDIX (Table S1). Some of the parameters were collected and calculated from literature and some were predicted by Simcyp calculators or obtained from Simcyp internal databases. We created a PO model for 30 mg OXY, an IV model for 0.1 mg/kg DZP and a PO model for 10 mg DZP according to the recommended dosages of the two drugs. In the PO OXY model, the absorption was described as a first order process, while in the PO DZP model, we utilized the ADAM absorption model implemented in the Simcyp software. For the IV DZP model, DZP was modeled to enter the systemic circulation by venous blood vessels. Experimental PK data extracted from the literature were used to verify our PBPK models, which include AUC, maximal concentration ( $C_{max}$ ) and  $T_{max}$ . Last, we compared different formulations of DZP interacts with OXY.

The observed and predicted PK data were listed in Table 4 and the Concentration-Time (CT) curves for OXY and DZP were depicted in Figure 10. From the Table 4 and Figure 9, we can see all the predicted AUC,  $C_{max}$  and  $T_{max}$  of OXY and DZP were within the range of their observed data (within the standard deviation (SD)), respectively. Because for the oral formulation of DZP we only collected data within 12 hours after the administration, our predicted CT PK data of PO DZP was correspondingly adjusted to 12 hours, i.e., we compared  $AUC_{12h}$  (the drug exposure from time zero to 12 hours) between predicted PO DZP and observed PO DZP.

**Table 4 The AUC,  $C_{max}$  and  $T_{max}$  of 30 mg PO OXY, 10 mg PO DZP and 1 mg/kg DZP.**

Dosing Strategy		AUC (SD) (ng·h/mL)	$C_{max}$ (SD) (ng/mL)	$T_{max}$ (SD) (h)
Oxycodone PO 30 mg (0-24 h)	Observed 1 <sup>a</sup>	268.2 (60.7)	39.3 (14.0)	2.6 (3)
	Observed 2 <sup>a</sup>	277.0 (89.6)	48.5 (15.9)	1.5 (NA)
	Predicted	311.83 (150.67)	38.0 (14.69)	1.2 (0.31)
Diazepam PO 10 mg (0-12 h)	Observed <sup>b</sup>	1530 (464.33)	317 (89.55)	1.32 (0.56)
	Predicted	1677.12 (434.66)	221.89 (51.5)	1.15 (0.35)
Diazepam IV 0.1 mg/kg (0-24 h)	Observed <sup>c</sup>	2198.5 (NA)	NA	NA
	Predicted	1932.46 (582.83)	NA	NA

SD is standard deviation and all units are shown in parenthesis. a: Observed 1 and Observed 2 are the experimental data collected from Drugs.com (<https://www.drugs.com>). b,c: Observed data for PO and IV DZP are respectively obtained from two reports ([80, 81]).

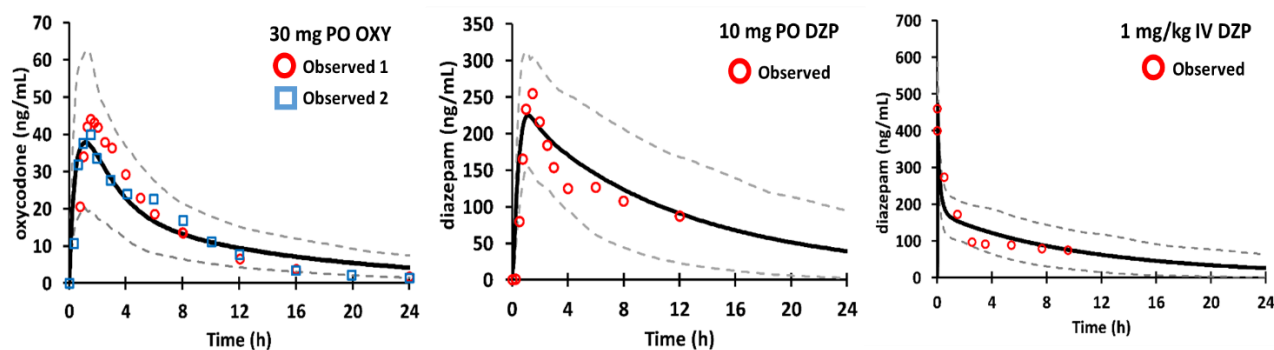


**Figure 9 The predicted concentration profiles of 30 mg PO OXY, 10 mg PO DZP and 1 mg/kg IV DZP and their observed data respectively.**

Red open circle and blue open squares represent the observed data. Black lines represent CT curve and Grey dashed lines represent the observed data. Black lines represent CT curve and Grey dashed lines represent 95% Confidence Interval of the population-based simulation of concentrations.

### 3.1.2.1 Competitive inhibition

Because usually the interaction between two different substrates with the same enzyme is competitive inhibition [82], we firstly hypothesize that diazepam is a competitive inhibitor of CYP3A4 and can inhibit the oxycodone which is predominately metabolized by CYP3A4. The  $K_i$  parameter of diazepam was calculated by Equation 8 and other input parameters have been listed in Table S1. DDI models for OXY and PO/IV DZP were built with the calculated  $K_i$  and the PK parameters as inputs. To better compare the DDI effect between OXY and DZP, we adjusted the dosage of diazepam from normal to overdose. The simulated concentration profiles of 30 mg OXY co-administered with different doses of PO/IV DZP are shown in Figure 10 and the predicted AUC Ratio and  $C_{max}$  Ratio of the DDI profiles with and without the presence of DZP were shown in Table 5.

**Table 5 The AUC Ratio and C<sub>max</sub> Ratio of the DDI profiles for PO OXY and 10 mg, 100 mg and 500 mg and 1000 mg of PO/IV DZP.**

Dosing Strategy	Formulation	AUC <sub>0-24h</sub> Ratio	CI[5%,95%]	C <sub>max</sub> Ratio	CI[5%,95%]
Oxycodone 30 mg + diazepam 10mg	PO	1.01	[1.00,1.01]	1.01	[1.00,1.01]
	IV	1.00	[1.00,1.01]	1.00	[1.00,1.00]
Oxycodone 30 mg + diazepam 100mg	PO	1.05	[1.03,1.07]	1.04	[1.02,1.06]
	IV	1.03	[1.02,1.05]	1.02	[1.01,1.04]
Oxycodone 30 mg + diazepam 500mg	PO	1.13	[1.09,1.19]	1.09	[1.06,1.14]
	IV	1.12	[1.07,1.17]	1.07	[1.04,1.12]
Oxycodone 30 mg + diazepam 1000mg	PO	1.20	[1.12,1.29]	1.12	[1.07,1.19]
	IV	1.18	[1.18,1.27]	1.10	[1.05,1.17]

CI is the 95% Confidence Interval. AUC<sub>0-24h</sub> Ratio is the exposure of AUC Ratio from the time zero to 24 hours.

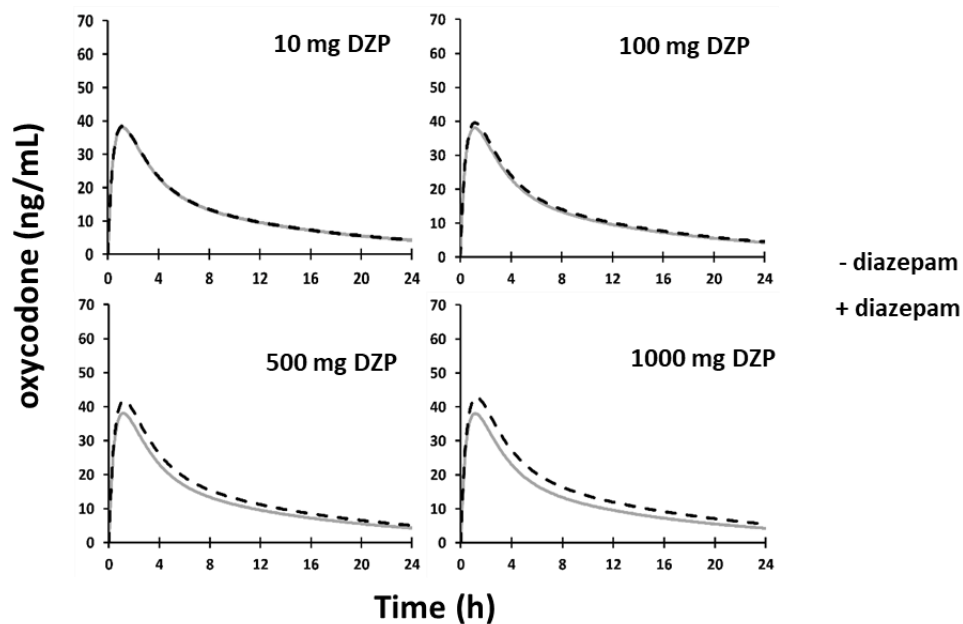


**Figure 10 The predicted concentration profiles of 30 mg oxycodone co-administered with 10 mg, 100 mg, 500 mg and 1000 mg DZP.**

The grey line represents the CT curve of OXY without the administration of DZP and the black dashed line represents the CT curve of OXY with the administration of DZP.

As shown in Figure 10, the accumulation of OXY concentration can only be observed when the dosage of PO DZP is 1000 mg. The plasma concentration of OXY increases with the administrated dosage of PO DZP increases, but the difference is not obvious for low doses of PO DZP. Correspondingly, the  $AUC_{24h}$  Ratio is only 1.01 and  $C_{max}$  Ratio is also 1.01 when treating with the normal dose of PO DZP. The AUC Ratio increases by 4.0% when the dose of PO DZP increases to 10 times the normal dose. Only when the dose of PO DZP was increased to 1000 mg, the simulated interaction between OXY and PO DZP can result in a growth of AUC of OXY by 1.20-fold and  $C_{max}$  of OXY by 1.12-fold. Similarly, the predicted DDI between OXY and IV DZP

causes only the increase of AUC by 1.18 folds and  $C_{max}$  by 1.10 folds for the largest DZP dose, which is even less obvious than PO OXY. The comparison of AUC Ratio for OXY with different administrations of DZP was shown in Figure 11. According to Figure 11, the simulated AUC Ratio of OXY with PO DZP is a little bit higher than with the same dosage of IV DZP.

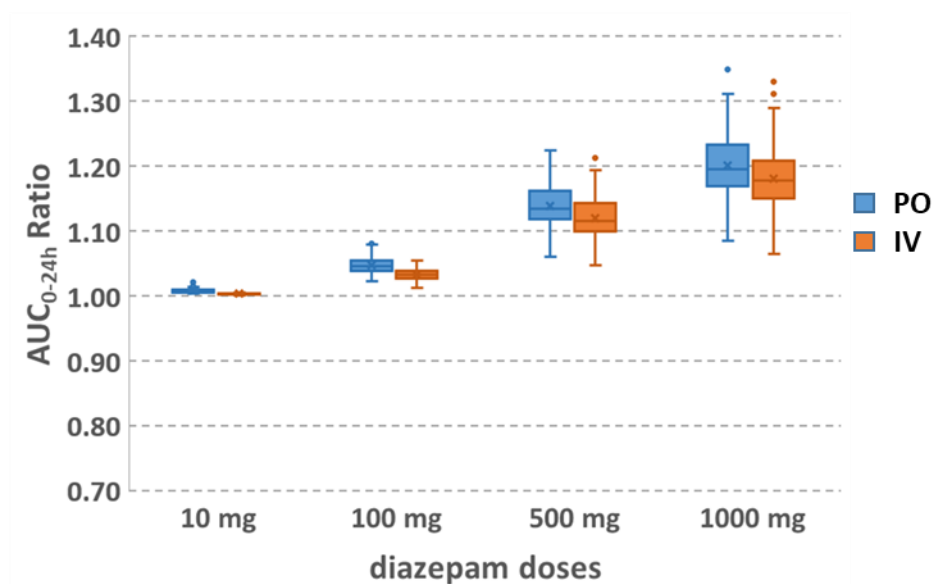


**Figure 11 The AUC<sub>0-24h</sub> Ratio of 30 mg OXY with the presence of 10 mg, 100 mg, 500 mg and 1000 mg of PO/IV DZP.**

The additional sensitivity analysis for  $K_i$  was also conducted in the DDI model between OXY and PO DZP by changing the  $K_i$  value from 0.165  $\mu\text{M}$  to 165  $\mu\text{M}$  in order to find out the significance  $K_i$  value influencing the simulation results and a surface plot which depicts the change of AUC Ratio of OXY with the change of  $K_i$  value of dosage of DZP was created (Figure 12). The corresponding AUC Ratio of DDI when concurrently taking 30 mg OXY and different dosage of

DZP changed from 1.000 to 1.375 in terms of  $K_i$  in the range 0.165-165. Accordingly, Figure 13 shows a series of C-T curves of oxycodone with the co-administration of 1000 mg diazepam when applying the different value of  $K_i$  to the DDI model.

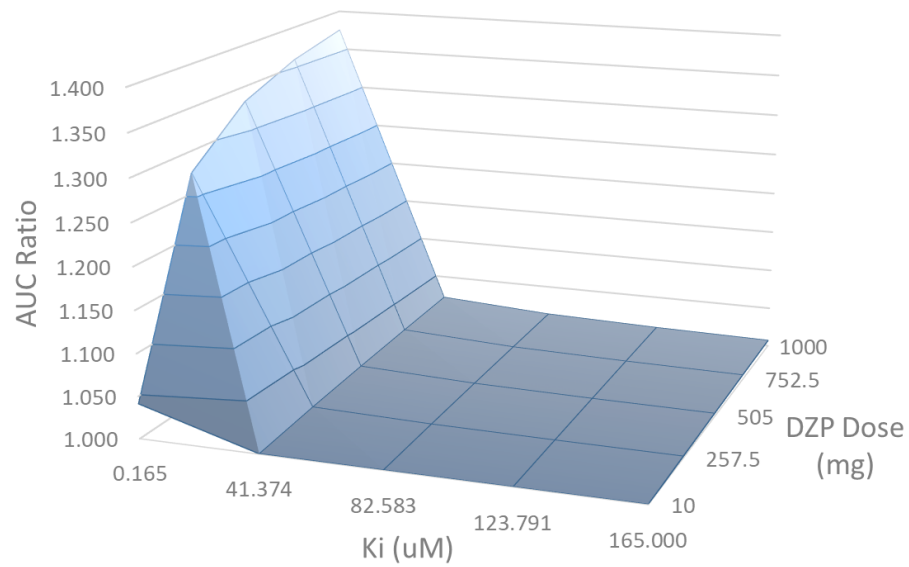


**Figure 12 The AUC Ratio of OXY with different dosage of PO DZP when  $K_i$  value is ranged in 0.165-165  $\mu\text{M}$ .**

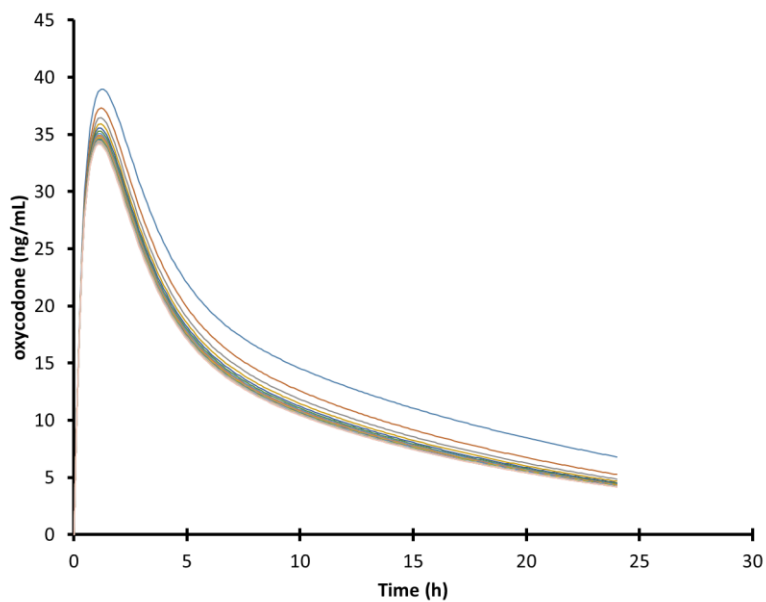


**Figure 13 A series of C-T curves of oxycodone in plasma with the presence of 1000 mg diazepam when applying  $K_i$  in range 0.165-165  $\mu\text{M}$ .**

### 3.1.2.2 Mixed type inhibition

Although it is believed competitive inhibition commonly happens between two substrates for the same enzyme, the interaction between CYP3A4 substrates is always complex. Therefore, we combined competitive inhibition with mechanism-based inhibition in modeling the DDI of OXY and PO DZP. The concentration of mechanism-based inhibitor associated with half-maximal inactivation rate ( $k_{app}$ ) and the inactivation rate of the enzyme ( $k_{inact}$ ) were listed in Table S1. The mechanisms of competitive and mechanism-based inhibitions have been described in the method section. The comparison of AUC Ratio of OXY with different dosage of PO DZP under the competitive inhibition and mixed-type inhibition respectively was shown in Figure 14. The detailed AUC Ratio of DDI profiles based on mixed-type inhibition was listed in Table 6. From the results, it is clear that the AUC and  $C_{max}$  both increase a little bit higher for the same doses of

DZP when applying the mixed-type inhibition than only utilizing competitive inhibition in the DDI model.

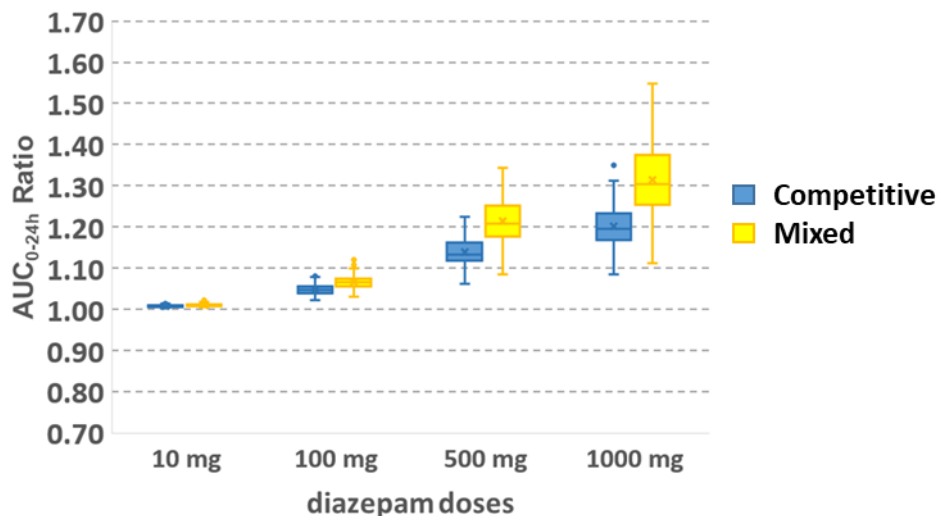


**Figure 14** The AUC<sub>0-24h</sub> Ratio of 30 mg OXY with the presence of 10 mg, 100 mg, 500 mg and 1000 mg of PO DZP when applying competitive inhibition and mixed-type inhibition.

**Table 6** The AUC Ratio and C<sub>max</sub> Ratio of the DDI profiles for PO OXY and 10 mg, 100 mg and 500 mg and 1000 mg of PO DZP when applying mixed-type inhibition to the DDI model.

Dosing Strategy	AUC <sub>0-24h</sub> Ratio	CI[5%,95%]	C <sub>max</sub> Ratio	CI[5%,95%]
oxycodone 30 mg + diazepam 10mg	1.01	[1.01,1.02]	1.01	[1.00,1.02]
oxycodone 30 mg + diazepam 100mg	1.07	[1.04,1.09]	1.04	[1.03,1.06]
oxycodone 30 mg + diazepam 500mg	1.21	[1.13,1.31]	1.10	[1.06,1.16]

oxycodone 30 mg + diazepam 1000mg	1.30	[1.17,1.48]	1.13	[1.07,1.22]
--------------------------------------	------	-------------	------	-------------

CI is the 95% Confidence Interval.  $AUC_{0-24h}$  Ratio is the exposure of AUC Ratio from the time zero to 24 hours.

### 3.1.2.3 Other opioids and benzodiazepines

Besides oxycodone and diazepam, we also create PBPK models for other opioids such as buprenorphine and fentanyl and benzodiazepines like alprazolam, midazolam and triazolam to explore the pharmacokinetic DDIs between these two kinds of drugs utilizing Simcyp software. The formulation of the presumed inhibitors, benzodiazepines are all through the oral administration route. Model validation including comparisons of PK parameters between observation and prediction as well as the simulation curves for parent drugs were listed in Table 7 (the results for OXY and DZP were summarized in Table 4) and shown in Figure 14. The input parameters are summarized in Table S3. We only considered the binding and inhibitory effect of parent drugs and the  $K_i$  value of each substrate/inhibitor (shown in Table S3) was also predicted by Glide docking. The predicted AUC,  $C_{max}$  and  $T_{max}$  of the two types of drugs are all within the ranges of overserved values, except for buprenorphine, for which the PK parameters are slightly off the observed ranges. The PK profiles of fentanyl are unavailable. Moreover, as shown in Figure 15, the observed C-T data of these drugs are also within the CI range (the upper and lower grey dashed lines) of the simulated Concentration-Time (CT) curves.

**Table 7 The AUC<sub>0-24h</sub>, C<sub>max</sub> and T<sub>max</sub> of 4 mg PO buprenorphine, 0.1 mg/kg mg PO fentanyl, 2 mg PO alprazolam, 15 mg PO midazolam and 0.25 mg PO triazolam.**

Dosing Strategy		AUC <sub>0-24h</sub> (SD) (ng·h/mL)	C <sub>max</sub> (SD) (ng/mL)	T <sub>max</sub> (SD) (h)
buprenorphine PO 4 mg	Observed <sup>a</sup>	23.89 (10.29)	3.31 (1.98)	0.71 (0.196)
	Predicted	<b>9.89</b>	3.83	<b>0.25</b>
fentanyl IV 0.1 mg/kg	Observed <sup>b</sup>	NA	NA	NA
	Predicted	180.29	NA	NA
alprazolam PO 2 mg	Observed <sup>c</sup>	NA	33 (10)	1.9 (1.4)
	Predicted	405.96	30.53	1.20
midazolam PO 15 mg	Observed <sup>d</sup>	221.76 (63.78)	95.17 (39.01)	0.69 (0.60)
	Predicted	233.49	75.72	0.64
triazolam PO 0.25 mg	Observed 1 <sup>e</sup>	7.01 (3.47)	2.02 (0.77)	0.96 (0.51)
	Observed 2 <sup>f</sup>	NA	3.0 (1.3)	1.25 (0.9)
	Observed 3 <sup>f</sup>	NA	2.3 (1.2)	1.25 (0.6)
	Predicted	7.91	2.00	0.99

SD is standard deviation and all units are shown in parenthesis. a: The report for buprenorphine PK [83]; b: The PK data of 0.1 mg/kg fentanyl was found in literature without PK properties like AUC [84]. c: It was found in the report [85]. d: Found in literature [86]. e: The PK profiles for young people when given with triazolam [87] f: The PK parameters for single dose of triazolam in men (observed 2) and women (observed 3).

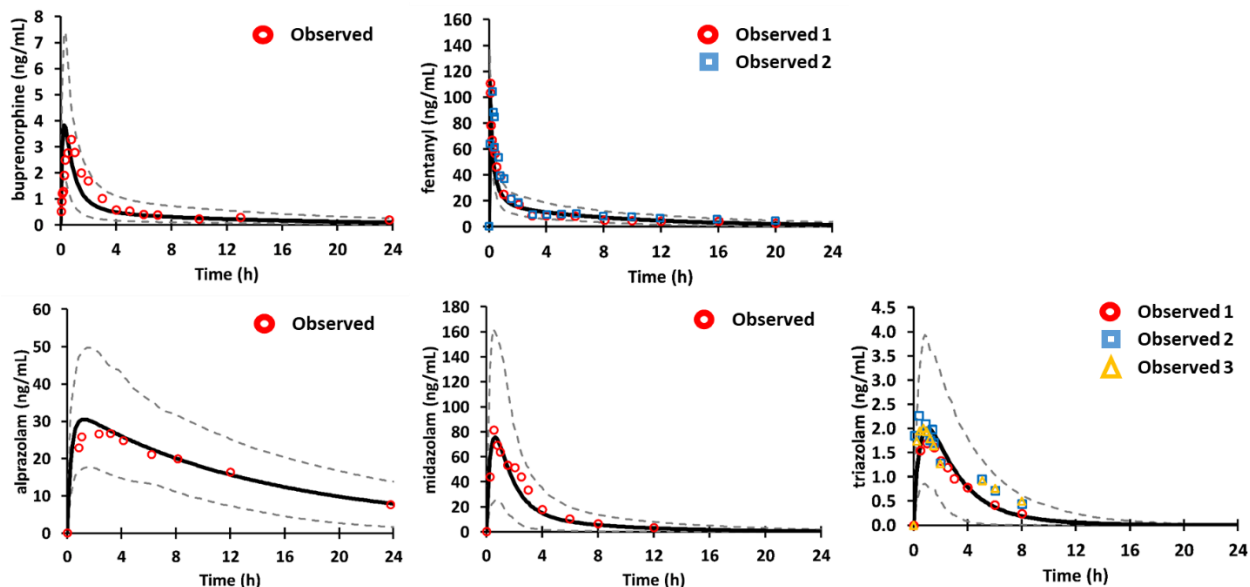


**Figure 15** The predicted concentration profiles of 4mg Sublingual (SL) buprenorphine, 0.1 mg/kg IV fentanyl, 2 mg PO alprazolam, 15 mg midazolam and 0.25 mg triazolam versus their observed data respectively.

Red open circle, blue open square and yellow open triangle represent the observed data. Black line represent CT curve and Grey dashed line represents 95% Confidence Interval of the population-based simulation of concentrations.

We also simulated the DDI simulations between opioids and benzodiazepines by assuming benzodiazepines are the competitive inhibitors of CYP3A4. The predicted AUC Ratios and  $C_{max}$  Ratios of DDI profiles were listed in Table 8 and the simulated opioids concentration profiles when concurrently taking normal/overdose of benzodiazepines were shown in Figure 16. To better compare the DDI effect of benzodiazepines, it is presumed that the normal dose of benzodiazepines is 10 mg and the amount of overdose is 1000 mg, while the dosage of opioids keeps normal. As shown in Table 8 and Figure 16, the fold change of AUC for oxycodone and fentanyl increased

significantly when taking with high dose of benzodiazepines. On the contrary, for buprenorphine, there was no obvious change in AUC even when the 1000 mg benzodiazepines is co-administered. In conclusion, the change of AUC ratio of fentanyl with normal or overdoses of benzodiazepines is significantly larger than that of oxycodone and buprenorphine.

**Table 8 The AUC Ratio and C<sub>max</sub> Ratio of the DDI profiles for normal dosage of opioids, including oxycodone (30 mg), buprenorphine (4 mg) and fentanyl (0.1 mg/kg) and benzodiazepines, including alprazolam, diazepam, midazolam and triazolam with normal (10 mg) and overdose (1000 mg), respectively.**

Opioids	Benzodiazepines	AUC <sub>0-24h</sub> Ratio (normal dose)	AUC <sub>0-24h</sub> Ratio (overdose)
oxycodone	alprazolam	1.03 [1.02,1.06]	1.37 [1.20,1.68]
	diazepam	1.01 [1.00,1.01]	1.20 [1.12,1.29]
	midazolam	1.00 [1.00,1.01]	1.08 [1.05,1.13]
	triazolam	1.01 [1.01,1.02]	1.23 [1.15,1.31]
buprenorphine	alprazolam	1.00 [1.00,1.00]	1.01 [1.01,1.03]
	diazepam	1.00 [1.00,1.00]	1.01 [1.00,1.01]
	midazolam	1.00 [1.00,1.00]	1.01 [1.00,1.01]
	triazolam	1.00 [1.00,1.00]	1.01 [1.01,1.02]
fentanyl	alprazolam	1.05 [1.03,1.08]	2.32 [1.85,2.76]
	diazepam	1.00 [0.99,1.03]	1.39 [1.22,1.55]
	midazolam	1.00 [1.00,1.01]	1.18 [1.09,1.26]
	triazolam	1.01 [1.01,1.03]	1.59 [1.37,1.81]

CI is the 95% Confidence Interval, which is within the brackets.  $AUC_{0-24h}$  Ratio is the exposure of AUC Ratio from the time zero to 24 hours.

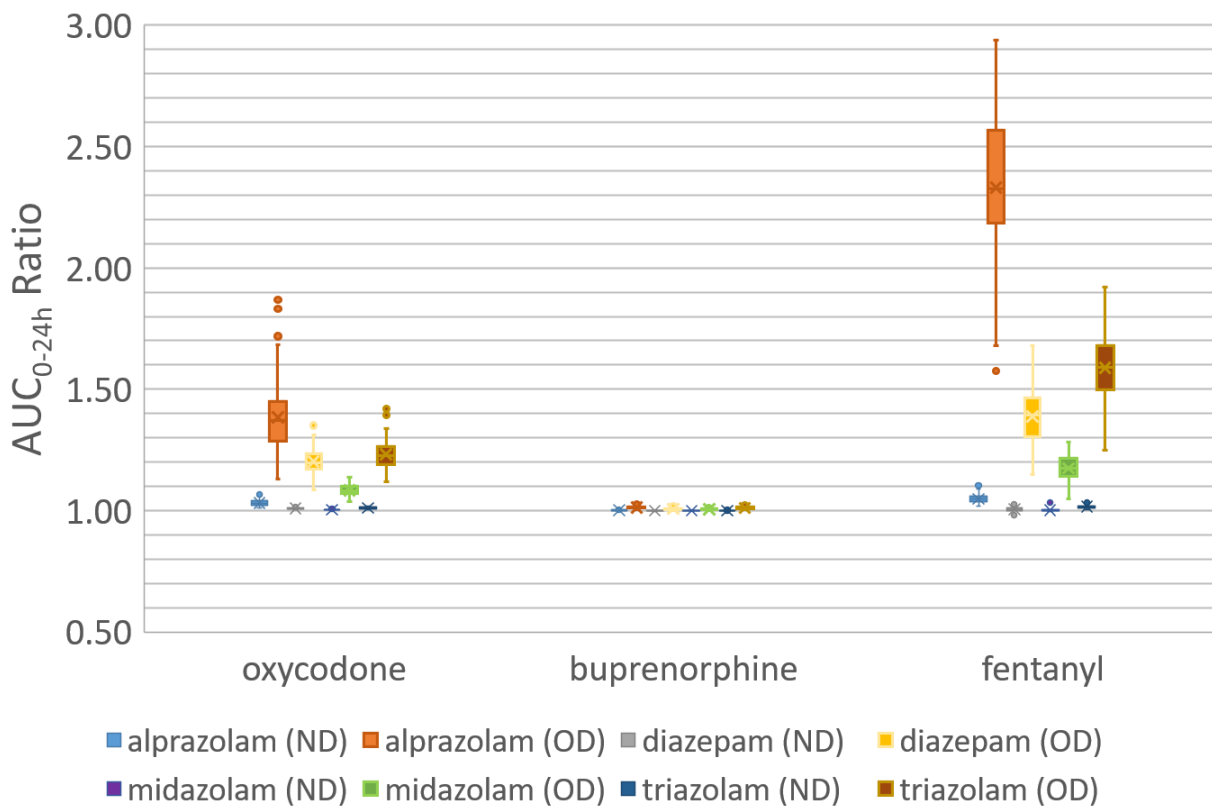


**Figure 16** The  $AUC_{0-24h}$  Ratio of oxycodone, buprenorphine and fentanyl with the presence of normal dose (ND) and overdose (OD) of four benzodiazepines.

**Discussion** The full PBPK model is probably the most complicated PBPK model existed currently, which consists of different organs in the human body linked by blood circulation. Different from the empirical PK models, there are multiple compartments in a PBPK model and the DDI modeling and simulation based on the PBPK models is closer to the real situation. In this study, we ignored

the transports in the DDI models because there is no report on any transport being shared by oxycodone and diazepam so far. We also ignored the inhibitory ability of metabolites given the fact that the concentration of metabolites of DZP is only approximately one-tenths of the concentration of the parent drug. The docking results showed that DZP had better binding affinity than OXY when binding with CYP3A4, so we predominantly studied the effect of DZP on OXY. The  $K_i$  value of DZP is a potential source of error as there is no exact experimental  $K_i$  value available and we only estimated the  $K_i$  value using the Glide docking score. The inaccurate  $K_i$  value may lead to wrong study conclusion, so to exclude the impact of  $K_i$  value for the DDI profiles, the sensitivity analysis was conducted by changing the calculated  $K_i$  from 1/10-fold to 100-fold to explore the impact of  $K_i$  value on AUC Ratio. As shown in Figure 12, the AUC Ratio changes only from 1.000 to 1.375 by changing the  $K_i$  value and dosage of DZP, indicating the error of  $K_i$  would not have a large influence on the DDI effect between two drugs. This finding can also be further illustrated in Figure 13, which implied that the PK interaction between OXY and DZP is very weak and does not have any clinical meaning since even though the  $K_i$  is very low and the dosage of DZP is very high (1000 mg), the exposure of OXY still did not have significant growth with the presence of DZP.

The correction of PBPK model of OXY and PO/IV DZP has been verified by comparing the PK properties of observed data and simulated data. Because the AUC,  $C_{\max}$  and  $T_{\max}$  of the predicted profiles of two drugs are all within the standard deviation range of the observed ones and the curves generally fit the experimental data well as demonstrated in Figure 10, the PBPK models are all credible. As for DDI profiles, it was found that there was no DDI between normal doses of OXY and DZP, but weak PK interaction between these two drugs when co-administering normal dose of OXY and overdose DZP. When the dose of DZP increases, its inhibitory effect on

the OXY becomes more obvious. The inhibitory ability of oral administration of DZP is slightly stronger than the IV administration DZP. The reason for causing this difference might be related to the relatively smoother change of PO DZP concentration since oral drug does not directly go into blood circulation while IV formulation dose. The transporter DDI was not considered in this model because there is lack of the clinical evidence that transporters, such as those found in blood-brain-barrier (BBB), causes significant interactions between the two types of drugs. Furthermore, the inhibitory effect of DZP is slightly larger when applying mixed-type inhibition to the DDI model, especially when the dosage of DZP is much higher than the normal dose. For example, the AUC Ratio in the mixed-type inhibition model is 1.30, which is 8.3% higher than the AUC Ratio in the pure competitive inhibition model.

According to the report in 2005 [88], the toxic concentration of OXY is 0.69 mg/L (690 ng/mL), which is much higher than the  $C_{max}$  of the 30 mg oxycodone when taking with even 1000 mg diazepam. This toxic concentration can only be achieved when taking around 500 mg oxycodone alone in terms of our PBPK model. The only problem is there is only one case of taking the dosage of diazepam over 1000 mg [89] and 1000 mg is too high and is lack of clinical meaning. According to the literature, when the plasma concentration of the diazepam was as high as 4792 ng/mL, patients were minimally sedated and were discharged within 24 h [76]. When the dosage of oral DZP is 200 mg, its maximal concentration is 4500 ng/mL. Obviously, PK interaction cannot be observed with the co-administration of 30 mg OXY and 200 mg DZP in terms of the AUC Ratio results in Table 9, indicating that there is almost no PK interaction between these two drugs.

Similarly, we also exchanged the role of OXY and DZP to see how OXY would affect the normal dose of DZP's metabolism. The opposite DDI simulation results are consistent with the

previous situation. The AUC Ratio of 10 mg DZP with the administration of 30 mg OXY is 1.01 and this value only limitedly changed to 1.07 when the dosage of OXY became 500 mg.

**Table 9 The AUC<sub>0-24h</sub> Ratio and C<sub>max</sub> Ratio of 30 mg OXY with the co-administration of 200 mg PO DZP (toxicity dosage).**

Dosing Strategy	AUC <sub>0-24h</sub> Ratio	CI[5%,95%]	C <sub>max</sub> Ratio	CI[5%,95%]
oxycodone 30 mg + diazepam 200mg	1.08	[1.05,1.11]	1.06	[1.04,1.09]

CI is the 95% Confidence Interval. AUC<sub>0-24h</sub> Ratio is the exposure of AUC Ratio from the time zero to 24 hours.

The simulated concentration profiles of three opioids and four benzodiazepines are mostly predicted well compared with the observed data as shown in Figure 15, Table 7 and Table 88, except for the AUC<sub>0-24h</sub> Ratio and T<sub>max</sub> of buprenorphine for which the predicted values were slightly out of the SD range of the observed data. As for DDI simulations, all four benzodiazepines showed larger inhibitory effects to oxycodone and fentanyl and the corresponding increase of AUC was generally larger for fentanyl than for oxycodone. This finding may be ascribed to the predicted liver fm<sub>3A4</sub> % (the contribution of CYP3A4 in the metabolism of drug) value of fentanyl is much higher for fentanyl (92.63%) than oxycodone (34.49%). There is almost no PK interaction between buprenorphine and benzodiazepines even the dose was set to 100 times of normal one because the fm<sub>3A4</sub> % of the drug is only 1.47% in liver.

### 3.1.3 Minimal PK modeling

The results of minimal PBPK modeling conducted by Simbiology were consistent with the results of empirical PK modeling using PySB and full PBPK modeling using Simcyp. The pharmacokinetic interaction between the two drugs is still not significant and it can only be observed when the oxycodone (OXY) is simultaneously taken with highly overdose diazepam (DZP).

The detailed structure of the PBPK model describing the ADME process and the interaction between OXY and DZP is illustrated in Figure 17. After oral doses and first-order absorption, OXY and DZP are separately absorbed into the portal vein compartments. The drugs then go to the liver compartments through the blood flow of portal veins ( $Q_{pv}$ ). In the liver, a part of OXY or DZP is metabolized and others enter the systemic blood compartment via the blood flows from the liver ( $Q_{H,o}$ ,  $Q_{H,d}$ ). In the systemic blood, these two drugs will be urinary eliminated in urine or go back to the portal vein via the blood flow of systemic blood ( $Q_{pv,o}$ ,  $Q_{pv,d}$ ). The only difference between OXY model and DZP is that we utilized a four-compartment brain model for OXY but a three-compartment model for DZP. We added an additional brain compartment for OXY because of its ability to cross the blood-brain barrier. DZP can easily cross blood-brain barrier because of its high lipid solubility and its relatively high fraction of plasma protein binding, so we do not need to add an additional compartment when constructing the minimal PBPK model for it. The clearances of entering and out of the brain ( $CL_{in}/CL_{out}$ ) for OXY are obtained from the literature [90].

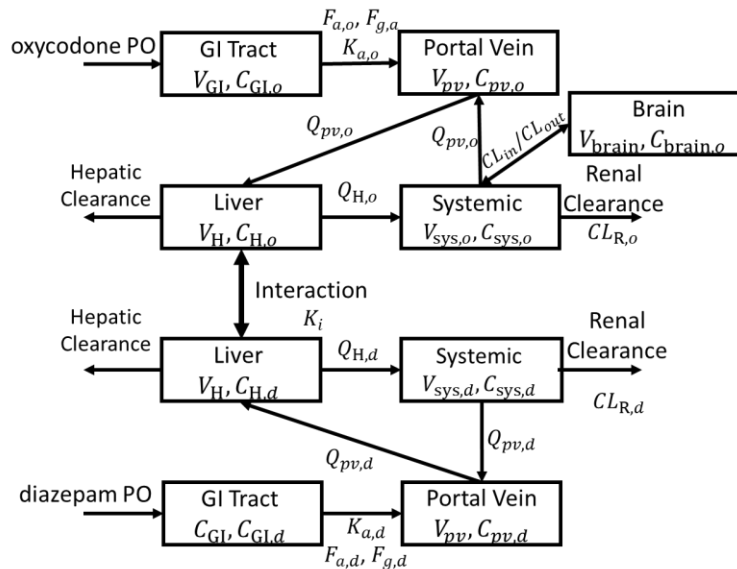


**Figure 17 The DDI model between OXY and DZP built using Simbiology.**

The  $V_{GI}$ ,  $V_{pv}$ ,  $V_H$ ,  $V_{brain}$  represent the volume of gastrointestinal (GI) tract, portal vein, liver and brain.  $F_{a,o}$ ,  $F_{g,a}$ ,  $K_{a,o}$ ,  $C_{pv,o}$ ,  $C_{H,o}$ ,  $V_{sys,o}$ ,  $C_{sys,o}$ ,  $C_{brain,o}$ ,  $CL_{R,o}$  are the fraction absorbed from the gastrointestinal tract, the gut availability, the absorption rate, the concentration in portal vein, the concentration in liver, the concentration in brain, the volume of distribution in systemic blood, the concentration in systemic blood, and the renal clearance of OXY, respectively.  $F_{a,d}$ ,  $F_{g,d}$ ,  $K_{a,d}$ ,  $C_{pv,d}$ ,  $C_{H,d}$ ,  $V_{sys,d}$ ,  $C_{sys,d}$ ,  $CL_{R,d}$  are DZP's respective values.  $K_i$  is the inhibitory constant of DZP.

The unbound intrinsic clearance mediated by CYP3A4 and CYP2D6 for OXY ( $CL_{int,o}$ ) is described by Equation 17, and comparatively, the intrinsic clearance mediated by CYP3A4 and CYP2C19 for DZP ( $CL_{int,d}$ ) is described by Equation 18. The corresponding metabolic pathways are shown in Figure 1-2.

$$(17) CL_{int,o} = \frac{CL_{int,NOC}}{1 + \frac{C_{H,d}}{K_i}} + CL_{int,OM}$$

$$(18) CL_{int,d} = CL_{int,TMZ} + CL_{int,NDZ}$$

Where  $CL_{int,NOC}$ ,  $CL_{int,OM}$ ,  $CL_{int,TMZ}$ ,  $CL_{int,NDZ}$  are the intrinsic clearance of metabolic pathways of noroxycodone (NOC) formation, oxymorphone (OM) formation, temazepam (TMZ) formation and nordazepam (NDZ) formation.

In terms of Figure 17, a series of processes in PBPK model previously described for OXY and DZP can be quantitatively described by the ordinary differential Equations below.

For OXY:

$$V_{abs,o} = k_{a,o} \cdot Dose(OXY) \cdot F_{a,o} \cdot F_{g,o} \cdot e^{-k_a t}$$

$$V_{pv} \frac{dC_{pv,o}}{dt} = Q_{sys} \cdot C_{sys,o} + V_{abs} - Q_{pv,o} \cdot C_{pv,o}$$

$$V_H \frac{dC_{H,o}}{dt} = Q_{pv} \cdot C_{pv,o} - \frac{Q_{H,o} \cdot C_{H,o}}{K_p} - \frac{f_{b,o} \cdot CL_{int,o} \cdot C_{H,o}}{K_p}$$

$$V_{sys,o} \cdot \frac{dC_{sys,o}}{dt} = \frac{Q_{H,o} \cdot C_{H,o}}{K_p} - Q_{sys,o} \cdot C_{sys,o} - f_{b,o} \cdot CL_{in,o} \cdot C_{sys,o} + f_{b,o} \cdot CL_{out,o} \cdot C_{brain,o} - CL_{R,o} \cdot C_{sys,o}$$

$$V_{brain} \frac{dC_{brain,o}}{dt} = f_{b,o} \cdot CL_{out,o} \cdot C_{brain,o} - f_{b,o} \cdot CL_{in,o} \cdot C_{sys,o}$$

For DZP:

$$V_{abs,d} = k_{a,d} \cdot Dose(DZP) \cdot F_{a,d} \cdot F_{g,d} \cdot e^{-k_{a,d} t}$$

$$V_{pv} \frac{dC_{pv,d}}{dt} = Q_{sys} \cdot C_{sys,d} + V_{abs,d} - Q_{pv,d} \cdot C_{pv,d}$$

$$V_{H,d} \frac{dC_{H,d}}{dt} = Q_{pv} \cdot C_{pv,d} - \frac{Q_{H,d} \cdot C_{H,d}}{K_p} - \frac{f_{b,d} \cdot CL_{int,d} \cdot C_{H,d}}{K_p}$$

$$V_{sys,d} \cdot \frac{dC_{sys,d}}{dt} = \frac{Q_{H,d} \cdot C_{H,d}}{K_p} - Q_{sys,d} \cdot C_{sys,d} - CL_{R,d} \cdot C_{sys,d}$$

Where  $V_{abs,o}$  and  $V_{abs,d}$  are the absorption velocities of OXY and DZP, respectively.  $CL_{int,o}$  and  $CL_{int,d}$  are derived using Equations 17 and 18 as mentioned before. All the parameters of PBPK model, which come from literature or are calculated using the relevant equations or are estimated using rational assumptions are collected in Table S2. For metabolites, only the parameters related to metabolic clearance are considered because according to the simulation results from full PBPK modeling, the concentrations of metabolites of OXY and DZP were around one-tenth of the concentrations of their own parent drugs and their effects were low.

The simulated concentration–time profiles for OXY and DZP in 24 hours are depicted in Figure 18 and the correspondingly PK parameters were listed in APPENDIX. Digital data was extracted from the experiment and was compared to the simulated curves. As shown in Table 10, the predicted AUC,  $C_{max}$  and  $T_{max}$  in this relatively simpler PBPK model are also within the error range of observed data as Simcyp did.

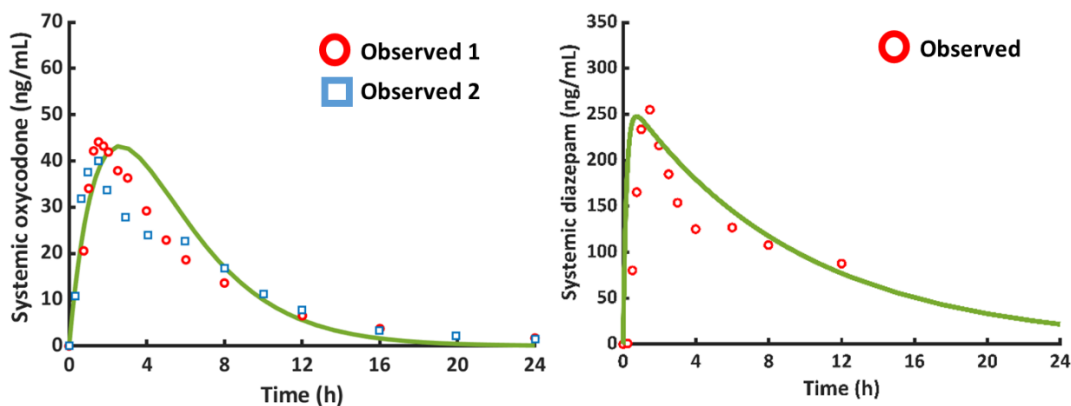


**Figure 18** The predicted concentration profiles of 30 mg PO OXY and 10 mg PO DZP as well as their observed data respectively by Simbiology.

Red open circle and blue open square represent the observed data. Green line represents simulation concentrations.

**Table 10** The simulated AUC,  $C_{max}$  and  $T_{max}$  of 30 mg PO OXY and 10 mg PO DZP.

Drug	AUC (ng·h/mL)	$C_{max}$ (ng/mL)	$T_{max}$ (h)
oxycodone	AUC <sub>0-24h</sub> : 308.05	43.01	2.5
diazepam	AUC <sub>0-12h</sub> : 1801.71	247.65	0.8

The similar strategy applied in full PBPK modeling by using Simcyp to explore the inhibitory effect of DZP on OXY was repeated to study the DDI between the two drugs using the minimal PBPK model shown in Figure 17. The OXY concentration became slightly higher when co-administered with DZP than OXY is administered alone. With the increased dose of DZP, the general concentration of OXY in plasma (systemic blood compartment) slightly increased. AUC Ratio in 24 hours was also calculated via the mathematical integration using Matlab and is listed

in Table 11. The change in AUC Ratio was very small and similarly, only when the concomitant dose of DZP being 100 times of the normal dose can cause the AUC Ratio changes from 1.00 to 1.27, rising about 27%. The change of OXY was depicted in Figure 19. To better compare the DDI simulation using minimal PBPK model in Simbiology and full PBPK model in Simcyp, we also calculated the correlation of AUC Ratios in the DDI profiles by the Pearson correlation coefficient [91] for these two methods and we found the two models have very high correlation (Figure 20).

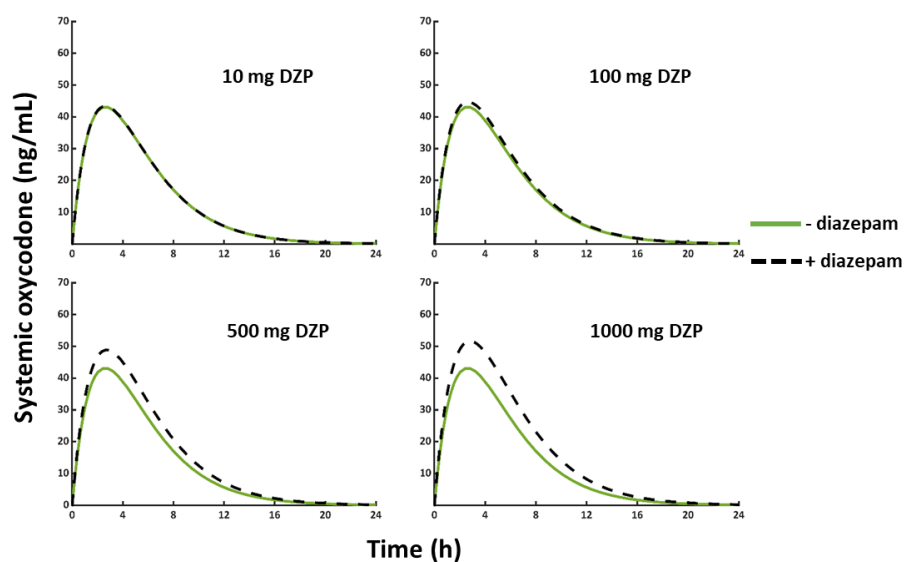


**Figure 19 The predicted concentration profiles of 30 mg oxycodone co-administered before and after 10 mg, 100 mg, 500 mg and 1000 mg DZP by Simbiology.**

The green line represents the CT curve of OXY without the administration of DZP and the black dashed line represents the CT curve of OXY with the administration of DZP.

**Table 11 The AUC Ratio and C<sub>max</sub> Ratio of the DDI profiles for PO OXY and 10 mg, 100 mg and 500 mg and 1000 mg of PO DZP when applying minimal PBPK model using Simbiology to construct the DDI model.**

Dosing Strategy	AUC <sub>0-24h</sub> Ratio	C <sub>max</sub> Ratio
oxycodone 30 mg + diazepam 10mg	1.00	1.01
oxycodone 30 mg + diazepam 100mg	1.04	1.04
oxycodone 30 mg + diazepam 500mg	1.17	1.14
oxycodone 30 mg + diazepam 1000mg	1.27	1.2

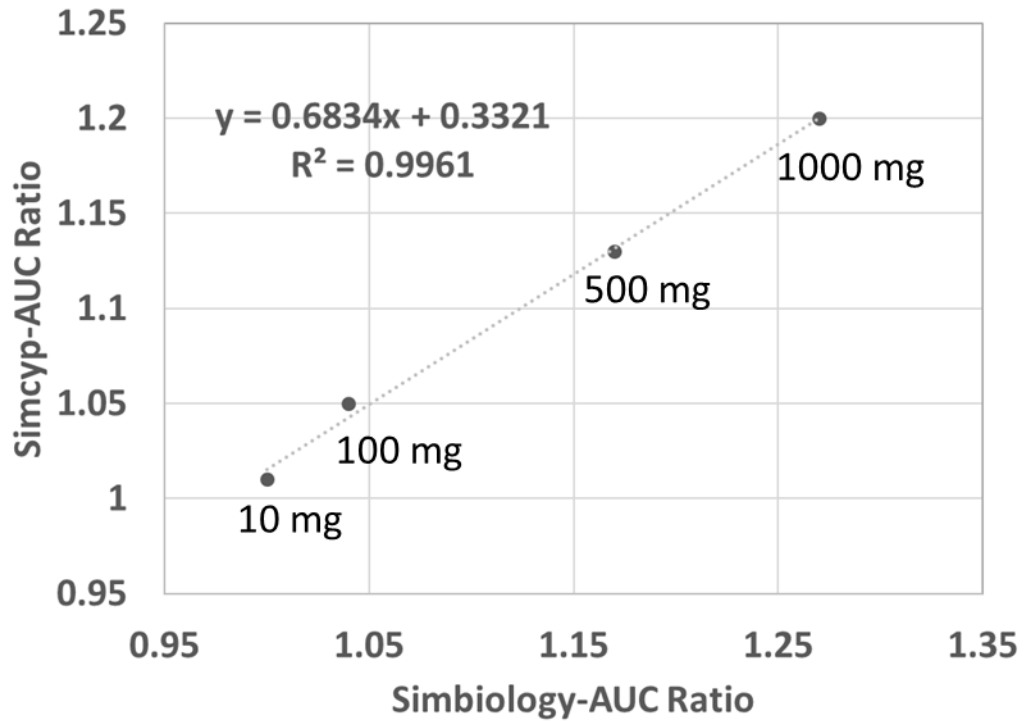


**Figure 20 The correlation between AUC Ratio of OXY when simultaneously taking with different dose of DZP obtained from Simcyp and Simbiology.**

**Discussion** The purpose of PBPK modeling by utilizing Simbiology is to compare the simulated results of DDI in the simpler minimal PBPK model with the DDI in a more complex full PBPK model using Simcyp. In Simbiology, we can freely build any models through the friendly interface or through Matlab coding. In that way, we can discard or simplify some less important components or processes which are usually lack of measured parameters and thus facilitate us to explore the DDI effect between two drugs. On the other hand, there are a large set of parameters behind even a minimal PBPK model in Simcyp. As such, we built the minimal PBPK models for OXY and DZP in Simbiology.

As shown in Figure 18 and Table 10, the PK properties such as AUC,  $C_{max}$  and  $T_{max}$  are within the error range of observed data and close to the predicted ones using Simcyp. Also, the simulated CT curve fits experimental data well, indicating the credibility of the minimal PBPK model. In addition, as for the DDI model between OXY and DZP which was created based on the minimal PBPK model of these two drugs, It has been shown that the simulated results of DDI with a minimal PBPK model using Simbiology were similar with those produced by a full PBPK model utilizing Simcyp (Figure 19 and Table 11). There high correlation of AUC Ratios of DDIs between the two PBPK models further validated the reliability of the DDI model generated with Simbiology.

The results above indicate that in certain cases building a minimal PBPK model is more efficient than a full PBPK model, especially when there is lack of experimental data since a minimal PBPK model is much more realistic than a one-compartment PK model and less complicated than a full PBPK model.

## 3.2 PHARMACODYNAMICS

To better investigate the pharmacodynamics DDI between opioids and benzodiazepines, we performed molecular docking, molecular dynamics (MD) simulation and MM/PBSA energy calculations step by step for set of opioids (oxycodone, buprenorphine, naltrexone, methadone) and benzodiazepines (alprazolam, diazepam, midazolam and triazolam) binding to both the  $\mu$ - and  $\kappa$ -opioid receptors.

### 3.2.1 Molecular docking

To predict the binding affinity between ligands and receptors as well as the features of the binding sites of models, docking analysis was performed on several ligands, including opioids and benzodiazepines towards  $\mu$ - and  $\kappa$ -opioid receptors. In the following, the  $\mu$ -opioid receptor and  $\kappa$ -opioid receptor were abbreviated as MOR and KOR, respectively. Among the opioids, oxycodone is the agonist of MOR and KOR [16]. Buprenorphine was reported as partial MOR [92] and also may have potent KOR antagonist activity [93]. Methadone acts as a MOR agonist with relatively higher intrinsic activity but lower affinity [94] and naltrexone was reported as the competitive antagonists at the MOR and the KOR [95]. The docking poses of opioids and benzodiazepines were shown in Figure 20 and the best docking score for each ligand was summarized in Table 12.

In Table 12, we can find that generally, the docking scores of oxycodone, buprenorphine and methadone binding to agonist-bound MOR and KOR, 5C1M and 6B73 are better than binding to antagonist-bound MOR and KOR, 4DKL and 4DJH. For naltrexone, the binding behavior are different for the two opioid receptors: for MOR, the docking score of the active conformation is

worse than the inactive conformation, while for KOR, the trend is just the opposite. Also, the difference between docking scores of these opioids binding to active and inactive MOR is a little smaller than the difference of the docking scores for KORs. As for benzodiazepines, all of four ligands have better docking results docking with agonist-bound MOR and KOR than docking with antagonist-bound receptors. Among them, diazepam shows best docking results binding with 5C1M (active MOR) while midazolam is the ligand which has the best docking score binding to 6B73 (active KOR). Figure 21 compares the docking poses of benzodiazepines binding to MORs and KORs with opioids, indicating that the binding modes of benzodiazepines are closer to opioid agonists when docking with agonist-bound receptors. It also shows that binding modes of benzodiazepines are obviously different from the docking poses of opioids in 4DJH (inactive KOR).

**Table 12 The docking results (kcal/mol) for opioids and benzodiazepines binding to both the active and inactive X-ray structures of MOR and KOR.**

Classification	Drug	5C1M (MOR) (Active)	4DKL (MOR) (Inactive)	6B73 (KOR) (Active)	4DJH (KOR) (Inactive)
Opioid	oxycodone	-6.377	-5.926	-7.198	-4.278
	buprenorphine	-6.463	-6.068	<b>-5.958</b>	<b>-5.362</b>
	methadone	-5.104	-4.759	-5.387	-4.329
	naltrexone	-6.000	-6.912	<b>-7.419</b>	<b>-6.450</b>
Benzodiazepine	alprazolam	-6.055	-6.022	-6.801	-5.024
	diazepam	-6.807	-6.382	-6.512	-5.007
	midazolam	-6.385	-5.801	-6.848	-4.806
	triazolam	-6.086	-5.974	-6.833	-5.194

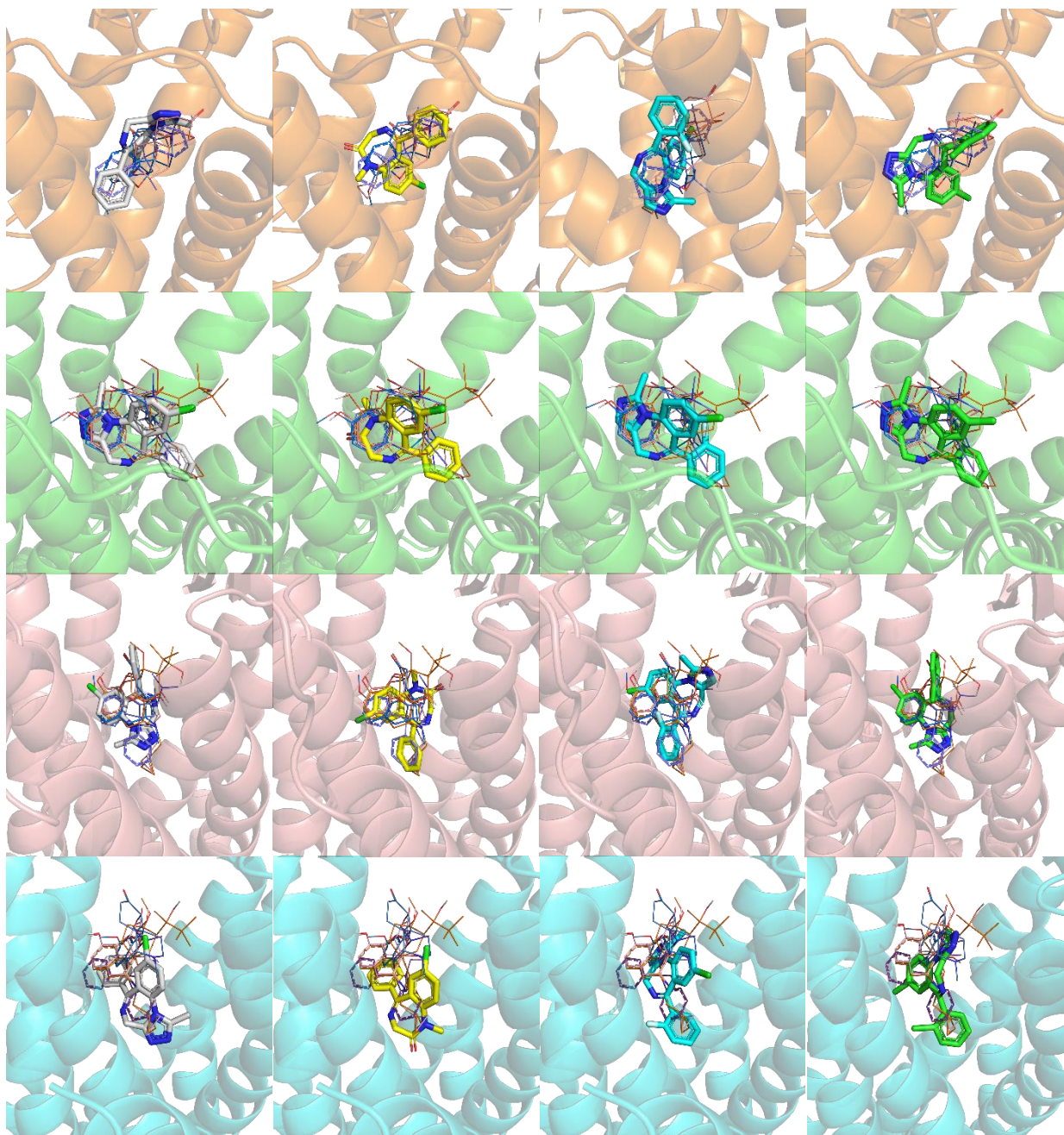


**Figure 21 The docking poses of opioids and benzodiazepines with opioid receptors.**

For receptors, orange protein represents 5C1M, green protein represents 4DKL, pink protein represents 6B73 and blue protein represents 4DJH. For ligands, benzodiazepines are shown as sticks and opioids are shown as lines. Benzodiazepines: alprazolam is white, diazepam is yellow,

midazolam is cyan and triazolam is green. Opioids: buprenorphine is orange, methadone is purple, naltrexone is pink and oxycodone is blue.

**Discussion.** As shown in Table 12, the docking results of opioids are mostly rational because opioids agonists (oxycodone, buprenorphine and methadone) showed relatively better docking scores when binding to the active opioid receptors than binding to inactive opioid receptors. However, some docking results conflict with the known facts. For example, naltrexone, a competitive antagonist of MOR and KOR, has illustrated a better binding affinity with 6B73, the active KOR compared with 4DJH (inactive KOR) according to docking scores. Buprenorphine, an antagonist of KOR turns out to have a better binding affinity to 6B73 rather than 4DJH, which is opposite to the known fact.

From docking results, we can infer that opioids and benzodiazepines have similar binding modes no matter the receptor is an active or inactive conformation. Furthermore, the docking scores for both opioids and benzodiazepines binding to the active conformation of KOR are much better than binding to the inactive structure, suggesting that these two kinds of drugs have similar mechanisms binding to KOR. It is our rational that diazepam can compete with oxycodone binding to KOR as an agonist or partial agonist. This finding could be further approved by the in-vitro study in 2001, exploring the potential interactions of benzodiazepines with cloned human opioid receptor subtypes and implying that three benzodiazepines, midazolam, chlordiazepoxide, and diazepam were agonists for KOR [96]. Glide docking also predicts that opioid agonists and benzodiazepines bind to the active structure of MOR better than to the inactive structure, although the differences of docking scores are smaller compared to KOR.

### 3.2.2 Molecular dynamics simulation

To investigate the dynamics of ligand binding, MD simulations were performed for four systems: active/inactive conformation of MOR and active /inactive conformation of KOR with opioids and benzodiazepines. The starting conformations of MOR/KOR in complex with ligands are from the best flexible docking poses. RMSD results for four systems are shown in Figure 22, respectively. Black curves represent the RMSDs of the backbone atoms of the whole opioid receptor protein, red curves represent the RMSDs of the backbone atoms of main chain atoms of the seven-transmembrane (7-TM); orange and purple curves respectively represent the RMSDs of opioids and benzodiazepines (BZD) fitting at their starting locations without considering their transition and rotation. On the other hand, the brown and blue curves represent the RMSDs of non-fitted opioids and benzodiazepines, considering not only their conformation changes but also their translocations and rotations through the MD simulations. The initial and the final average structures of each complex are shown in Figure 23. The initial complexes are grey and average conformations of opioid complexes and benzodiazepine complexes are orange and purple, respectively. The name of each ligand was abbreviated in three letters (OXY: oxycodone, BUP: buprenorphine, MET: methadone, NAT: naltrexone, APZ: alprazolam, DZP: diazepam, MDZ: midazolam, TRZ: triazolam).

In MOR (active/inactive) systems, RMSD results of all fitted opioids are low and stable. Among them, there is an increase of RMSD of non-fitted methadone in 5C1M (active) opioid receptor system after around 70 ns. The RMSD values of non-fitted BUP and NAT are less stable in 4DKL (inactive) system compared to 5C1M system though the RMSD of NAT became stable after 50 ns. As for benzodiazepines, the RMSD results of fitted APZ, MDZ and TRZ are all low

and stable except for fitted DZP, showing the fluctuation of RMSD values. The RMSDs of non-fitted benzodiazepines are all high (4-6 Å) and unstable in MOR systems except MDZ, which indicated relatively stable and lower RMSD values (2 Å) in 4DKL system. The position deviations as well as the conformation changes of all ligands in MOR systems (Figure 23) were consistent with the RMSD results.

As for KOR (active/inactive) systems, the RMSDs of opioids and their corresponding KORs are all stable the values for fitted ligands are all less than 2 Å. Particularly, the RMSD of fitted BUP binding with 6B73 (active) receptor is slightly higher and less stable than it binding to 4DJH (inactive) receptor. Furthermore, the RMSD curves of non-fitted MET and NAT are much more stable binding to 6B73 than binding with 4DJH. As for benzodiazepines, there are obvious fluctuations in the RMSD changes of non-fitted ligands as well as their corresponding receptors in 4DJH system. Generally, the RMSD results are relatively better for them in 6B73 system. The position deviations as well as the conformation changes of all ligands in KOR systems (Figure 23) were consistent with the RMSD results.

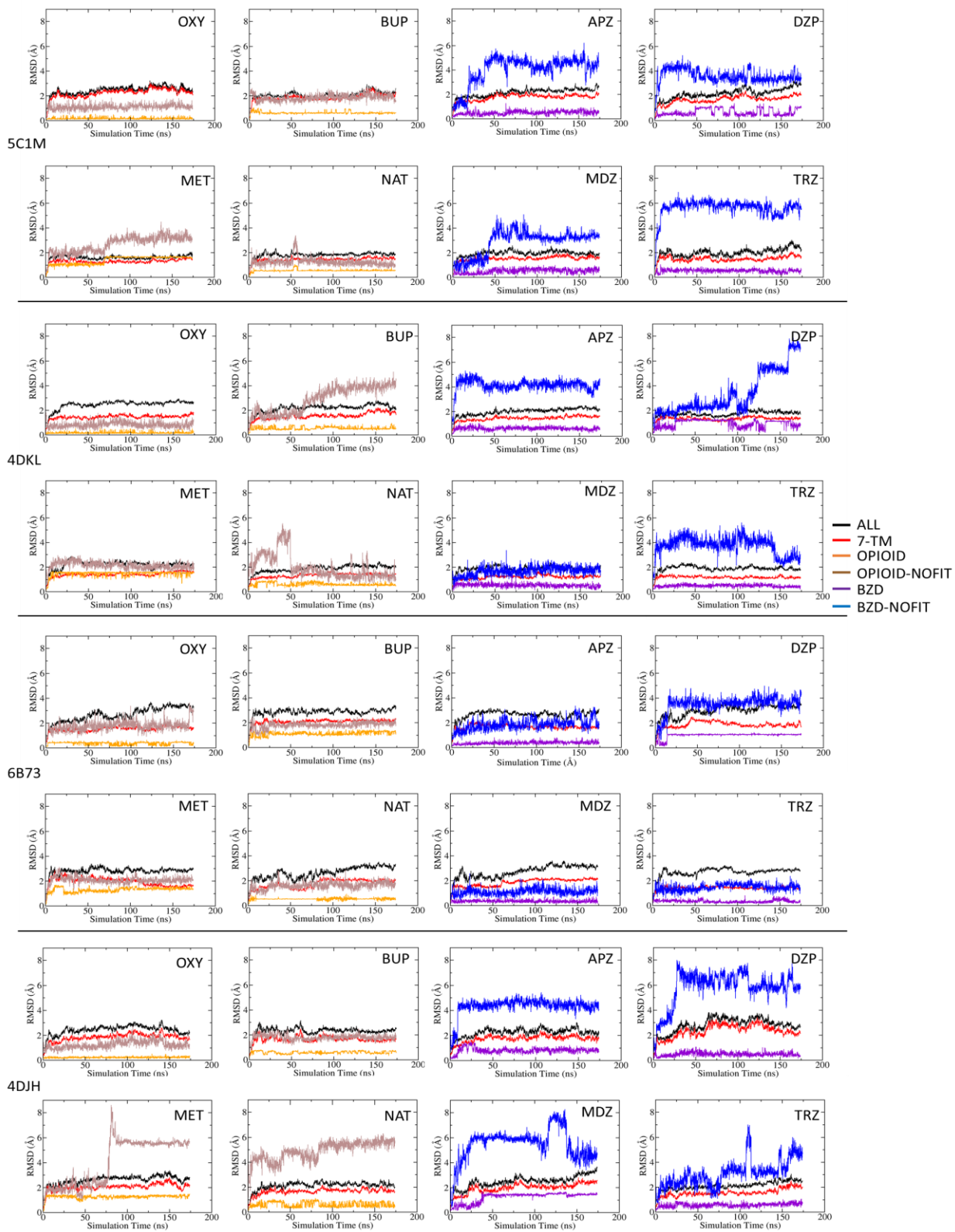
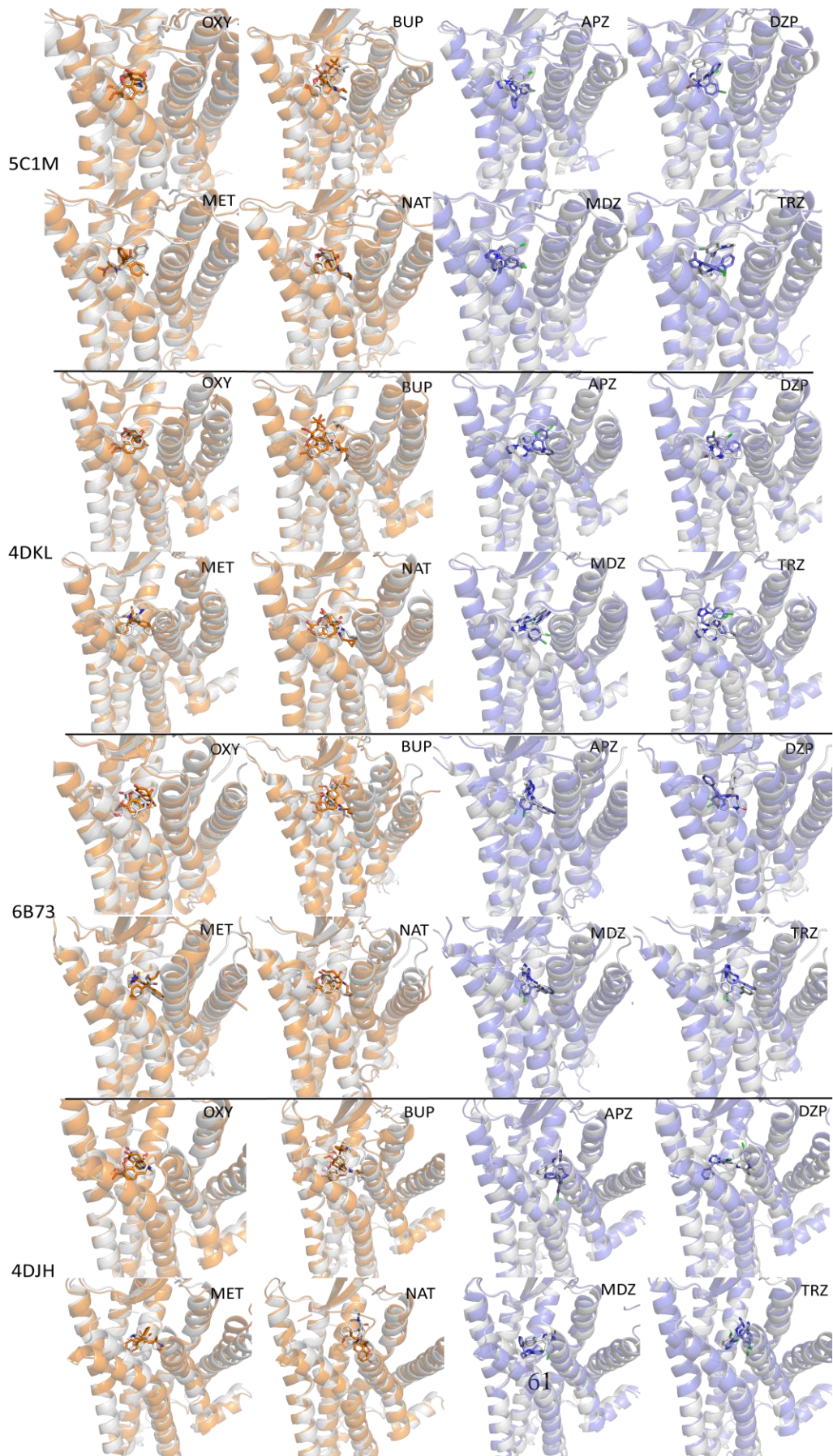


Figure 22 The RMSD results in the MD trajectories of MOR and KOR system.



**Figure 23 The comparison of the crystal structure (in grey) with the MD structure (in orange (opioids) and in purple (benzodiazepines)) in the MOR and KOR systems.**

**Discussion** In the MOR system, the binding modes for opioids are generally stable according to RMSD results. Although there is position deviation for MET in 5C1M system, indicating there might be two binding modes for the ligand. In addition, there are also position changes and rotations for BUP and NAT in 4DKL system. The conformations changed little for fitted APZ, MDZ and TRZ in MOR systems while they experienced translocations and rotations binding with MOR except for MDZ. Particularly, the non-fitted MDZ showed more stable binding mode compared with other benzodiazepines. The conformation and position for DZP both changed more than other benzodiazepines when binding with 5C1M and 4DKL receptors in the MD simulation. As for in the KOR system, the binding modes for opioids are also stable in terms of RMSD results in Figure 21 and structure comparisons in Figure 23. There were rotations and translocations for non-fitted MET and NAT binding with 4DJH receptor, which were consistent with their docking results. Benzodiazepines showed high binding selectivity for KOR since their conformations and locations changed much less when binding to the agonist-bound opioid receptor (6B73) than antagonist-bound opioid receptor (4DJH) according to the RMSD results as well as the comparisons between their crystal structures and average structures.

### **3.2.3 MM/PBSA calculations**

Binding free energy of each ligand was predicted using data from MD simulations and MM-PBSA binding free energy compositions were calculated after the trajectories were stabilized. The calculated binding free energies as well as the detailed contribution of different energy

compositions for four systems are presented in Table 13. To better compare the calculated binding affinities of each ligand, the binding free energies ( $\Delta G_{MM/PBSA}$ ) for all ligands in four systems were put together in Figure 24.

By comparing the MM/PBSA calculated energies for each ligand, totally, in the MOR systems, the comparisons of relative results within opioids and benzodiazepines are consistent with the docking results in 5C1M except for DZP. Its binding affinity with 5C1M receptor is much lower compared to other ligands. In 4DKL system, all benzodiazepines showed much lower measured binding energies compared with the binding modes of opioids. The comparisons of relative results between active conformation of MOR and inactive conformation of MOR are consistent with the docking scores, excluding OXY and NAT. Furthermore, the binding energies for BUP, MET and NAT are all lower in 5C1M system than in 4DKL system except for OXY. The calculated binding energy of OXY is -1.13 kcal/mol binding with 5C1M, which is higher than the energy, -4.97 kcal/mol when binding to 4DKL. All benzodiazepines showed much lower measured binding energies when binding with 5C1M compared to 4DKL.

As for KOR systems, DZP and TRZ have relatively higher binding energies binding with 6B73 (4.12 kcal/mol and 5.33kcal/mol) compared with other ligands in the same 6B73 system. In 4DJH system, all ligands, including opioids and benzodiazepines, have relatively higher binding free energies except for OXY and MDZ. If we compared the results between 6B73 and 4DJH systems, OXY also showed higher binding affinity in 4DJH system compared with in 6B73 system, while the measured energies for other opioids are lower in 6B73 system. For benzodiazepines, except for DZP, whole calculated energy is 4.12 kcal/mol in 6B73 but 1.82 kcal/mol in 4DJH, others' energies are all lower when binding with 6B73.

Because it is not clear that which energetic factors determine the total binding free energy, we compared correlations between the calculated binding free energies and each component of the calculated binding free energies and the correlation coefficient for them in four systems were listed in Table 14. It was found that the van der Waals energy (5C1M:  $r^2=0.8888$ , 6B73:  $r^2=0.8958$ ) and polar solvation free energy (5C1M:  $r^2=0.4406$ , 6B73:  $r^2=0.5325$ ) have better correlations for opioids in both 5C1M and 6B73 system. Furthermore, the non-polar solvation free energy has the best correlation for benzodiazepines in KOR systems (5C1M:  $r^2=0.6106$ , 6B73:  $r^2=0.6836$ ).

To better validate the results of MM/PBSA calculated results, we also found some experimental  $K_i$  values for opioids to help compare the relative values of binding free energies.  $K_i$  values can be transferred to binding free energy by Equation (4) and Equation (8) and the values of  $K_i$  as well as the experimental and predicted free energies were shown in Table 15. The  $K_i$  values for each ligand are all for active conformation of opioid receptors except MET, whose  $K_i$  value is for inactive conformation of MOR. All the  $K_i$  values were obtained from the experiments in rats. Because the experimental data of MET is for the inactive conformation of MOR, we only compared the experimental and calculated data within OXY, BUP and NAT. It seems that BUP has the lowest binding free energy no matter when binding with MOR or KOR. In addition, in both MOR and KOR systems, the difference of binding free energies between OXY and NAT is inconsistent between their own experimental and calculated data. Since OXY showed lower calculated binding free energy when binding to opioid receptors than NAT but higher experimental binding free energy compared with NAT.

**Table 13** Calculated binding free energies (kcal/mol) for individual terms using the MM/PBSA method.

Ligand	$\Delta E_{vdw}$	$\Delta E_{ele}$	$\Delta G_p^{sol}$	$\Delta G_{np}^{sol}$	$T\Delta S$	$\Delta G_{MM/PBSA}$
5C1M (Active MOR)						
<b>OXY</b>	-43.70±0.21	-23.72±0.17	46.33±0.01	-2.96±0.01	-21.50±0.09	-2.56±0.16
<b>BUP</b>	-58.24±0.16	-12.04±0.29	46.75±0.40	-4.80±0.01	-23.75±0.08	-4.57±0.21
<b>MET</b>	-41.51±0.17	-4.02±0.18	24.65±0.09	-3.52±0.00	-21.44±0.04	-2.97±0.05
<b>NAT</b>	-42.15±0.18	-14.40±0.16	36.85±0.28	-3.38±0.01	-20.80±0.03	-2.29±0.14
<b>APZ</b>	-36.36±0.05	-15.38±0.38	33.95±0.47	-3.00±0.01	-19.11±0.10	-1.67±0.14
<b>DZP</b>	-30.92±0.14	-4.83±0.10	21.15±0.14	-2.86±0.02	-18.61±0.03	1.15±0.16
<b>MDZ</b>	-36.85±0.22	-7.95±0.19	27.52±0.33	-3.15±0.01	-19.66±0.05	-0.77±0.19
<b>TRZ</b>	-35.68±0.08	-7.70±0.07	25.27±0.04	-3.10±0.01	-19.21±0.04	-2.00±0.03
4DKL (Inactive MOR)						
<b>OXY</b>	-42.64±0.22	-19.12±0.60	38.66±0.51	-2.87±0.01	-21.25±0.05	-4.72±0.18
<b>BUP</b>	-51.14±0.05	-7.96±0.31	38.96±0.15	-4.14±0.01	-22.61±0.04	-1.67±0.12
<b>MET</b>	-38.93±0.21	-1.75±0.32	21.14±0.24	-3.11±0.01	-20.75±0.02	-1.91±0.25
<b>NAT</b>	-42.23±0.27	-17.33±0.24	42.40±0.35	-3.19±0.01	-20.65±0.03	0.29±0.11
<b>APZ</b>	-40.85±0.17	-8.01±0.13	37.57±0.22	-3.01±0.01	-19.78±0.03	5.49±0.36
<b>DZP</b>	-34.94±0.14	-10.12±0.11	32.75±0.14	-2.77±0.00	-19.27±0.07	4.19±0.13
<b>MDZ</b>	-33.04±0.14	-4.31±0.25	25.85±0.37	-2.91±0.01	-18.54±0.05	4.12±0.04
<b>TRZ</b>	-31.04±0.12	-10.20±0.11	31.27±0.32	-2.82±0.00	-18.10±0.04	5.32±0.25
6B73 (Active KOR)						
<b>OXY</b>	-40.47±0.17	-1.37±0.46	23.94±0.51	-3.18±0.01	-19.96±0.01	-1.13±0.29
<b>BUP</b>	-59.24±0.12	-4.11±0.19	38.53±0.40	-4.69±0.01	-24.39±0.01	-5.13±0.44
<b>MET</b>	-40.78±0.16	-0.21±0.16	19.90±0.08	-3.29±0.01	-20.82±0.03	-3.55±0.36
<b>NAT</b>	-43.66±0.09	-3.39±0.28	30.21±0.09	-3.36±0.01	-20.59±0.04	0.39±0.29
<b>APZ</b>	-38.30±0.21	6.77±0.25	13.58±0.23	-3.11±0.01	-19.29±0.05	-1.77±0.25
<b>DZP</b>	-36.56±0.18	-2.21±0.23	26.08±0.16	-2.97±0.01	-19.79±0.06	4.12±0.18
<b>MDZ</b>	-40.45±0.07	0.26±0.15	19.57±0.17	-3.10±0.01	-20.25±0.04	-3.47±0.07
<b>TRZ</b>	-41.93±0.15	5.77±0.16	24.11±0.50	-3.21±0.01	-20.58±0.03	5.33±0.48
4DJH (Inactive KOR)						
<b>OXY</b>	-42.84±0.18	-5.61±0.23	25.54±0.43	-2.84±0.00	-20.78±0.01	-4.97±0.29

<b>BUP</b>	-57.44± 0.10	-0.78±0.22	43.94±0.17	-4.50±0.01	-24.82±0.03	6.05±0.04
<b>MET</b>	-33.04±0.04	1.23±0.02	19.07±0.16	-3.19±0.01	-18.93±0.04	3.00±0.15
<b>NAT</b>	-40.26±0.19	-11.22±0.10	40.81±0.35	-3.09±0.00	-20.28±0.06	6.51±0.12
<b>APZ</b>	-42.87±0.10	8.68±0.10	24.50±0.30	-2.96±0.01	-20.34±0.03	7.68±0.21
<b>DZP</b>	-32.47±0.05	-7.29±0.07	25.11±0.18	-2.75±0.01	-19.22±0.01	1.82±0.20
<b>MDZ</b>	-34.68±0.25	-1.94±0.21	17.51±0.10	-2.79±0.01	-18.96±0.04	-2.93±0.12
<b>TZ</b>	-34.39±0.21	-4.62±0.11	30.25±0.39	-3.12±0.01	-19.04±0.05	7.16±0.26

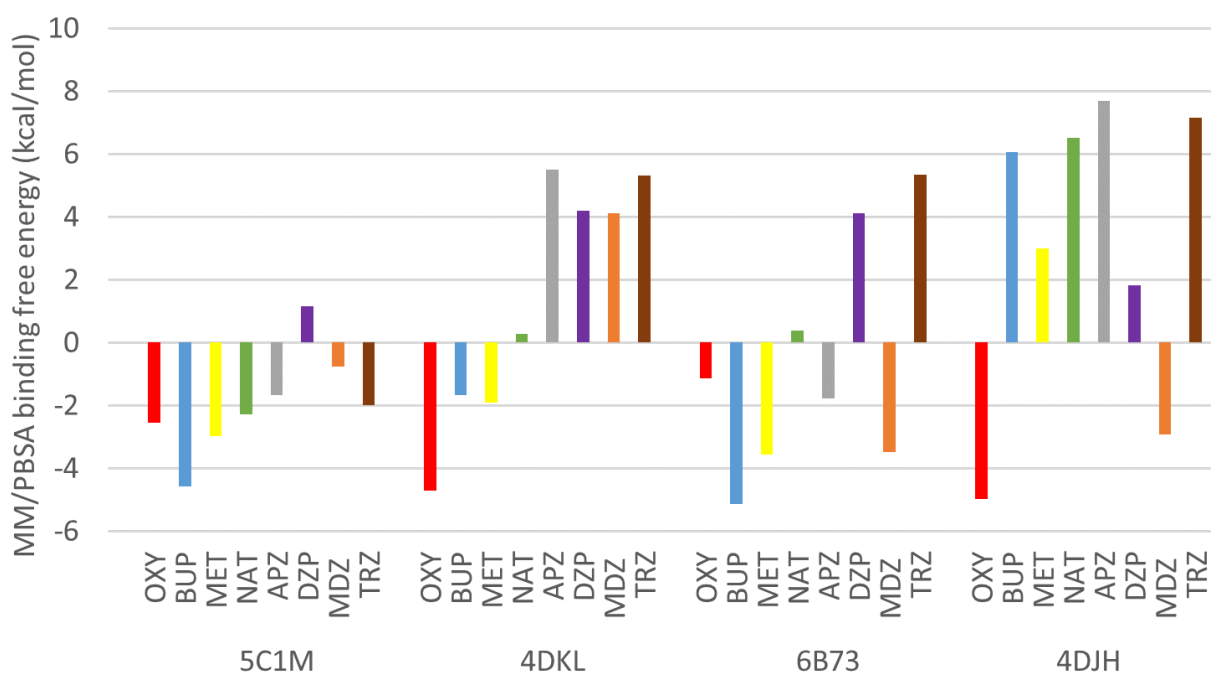


**Figure 24** Binding free energy ( $\Delta G_{MM/PBSA}$ ) for each ligand in MOR and KOR systems.

**Table 14 The correlation coefficients between calculated binding free energies and different components of energies.**

System	Classification	$\Delta E_{vdw}$	$\Delta E_{ele}$	$\Delta G_p^{sol}$	$\Delta G_{np}^{sol}$
<b>5C1M</b>	Opioid	0.8888	0.0823	0.1204	0.8958
	Benzodiazepine	0.7310	0.4047	0.4588	0.5062
<b>4DKL</b>	Opioid	0.0023	0.0348	0.0141	0.1162
	Benzodiazepine	0.1317	0.1569	0.2821	0.3096
<b>6B73</b>	Opioid	0.4406	0.0026	0.0947	0.5325
	Benzodiazepine	0.0002	0.0018	0.6106	0.0012
<b>4DJH</b>	Opioid	0.0493	0.001	0.3923	0.3229
	Benzodiazepine	0.2895	0.1736	0.6836	0.6267

**Table 15 The experimental  $K_i$  values ( $\mu\text{M}$ ) as well as the experimental and calculated binding free energies (kcal/mol) (Exp energy and Calc energy) for opioids.**

Ligand	MOR			KOR		
	$K_i$	Exp energy	Calc energy	$K_i$	Exp energy	Calc energy
OXY	0.0436 [97]	-10.04	-2.56	2.658 [97]	-7.61	-1.13
BUP	0.00013 [98]	-13.49	-4.57	0.000089 [98]	-13.71	-5.13
MET	0.110 [99] (Inactive)	-9.49	-1.91	NA	NA	-2.97 (active)/ -1.91 (inactive)
NAT	0.00046 [100]	-12.74	-2.29	0.00107 [100]	-12.24	0.39

**Discussion** Because the results of MM/PBSA are different between different systems, generally, we only compared the relative binding free energy of each ligand in the same system. In MOR systems, especially in 5C1M system, DZP showed lower binding affinity compared with other opioids and benzodiazepines while OXY has higher affinity. This result is consistent with the

corresponding RMSD result. In addition, benzodiazepines only showed slightly higher binding free energies than opioids when binding with 5C1M, the active conformation of MOR, but much higher binding free energies than opioids binding to 4DKL, the inactive conformation of MOR, indicating benzodiazepines have selectivity to MOR and might be the agonist of MOR. In KOR systems, APZ and MDZ showed relatively lower binding free energies in 6B73 system. But in 4DJH system, the binding affinity of APZ became lower compared to opioids though MDZ still have relatively higher binding affinity. DZP and TRZ both illustrated lower binding affinity when binding to agonist-bound KOR.

As shown in Table 14, in active conformations of MOR and KOR systems, van der Waals energy as well as the polar solvation energy of opioids are engaged in the determination of calculated binding free energy, while non-polar solvation energies of benzodiazepines contribute relatively more towards their calculated binding free energies, which indicated that polar factor is more important for the binding mode of opioids and non-polar factor is the predominant role for benzodiazepines.

However, generally there are some problems for our molecular modeling results: Currently we only considered the top one docking pose for each complex but sometimes there are two or more binding poses which are all appropriate for each ligand. Also, we should run multiple MD simulations with the consideration of multiple trajectories, but now we only consider one of them. In addition, metabolites of two kinds of drugs should be considered in PD interaction study. Moreover, the kinetics of receptor-ligand binding may play a more important role than binding affinity leading to PD interactions.

In the future, we will run more MD simulations for more distinct docking poses and study how active metabolites bind to the two opioid receptors. Since these metabolites may have better

effect on the opioid receptors than parent drugs do. Efficacy is also another important essential point which should be considered in the future because for some drugs (methadone), although they have low binding affinity for the receptors, their efficacy is very high, and this phenomenon can be explained by the binding kinetics which can be studied by nonequilibrium MD simulations.

Actually, the PD interaction is an ongoing project since besides additive PD interaction, other mechanisms can also contribute to the PD interactions between opioids and benzodiazepines. For example, synergetic effects on the same signaling pathways caused by both opioids and benzodiazepines in terms of their targets, so further research for these two types of drugs is needed in the future.

## **4.0 SUMMARY AND CONCLUSIONS**

### **4.1 PHARMACOKINETICS**

All three models we created for DDI between oxycodone (OXY) and diazepam (DZP), including empirical PK model, full PBPK model and minimal PBPK model, have achieved similar pharmacokinetic DDI effects. There is no PK interaction between the normal dose of OXY and DZP, but DDI can be expected to exist with a highly overdose of diazepam. The inhibitory effect of oral administration of DZP for OXY is slightly higher than the IV administration. All models predict that the PK contributes little to the DDI between OXY and DZP, even though the inhibitory effect of DZP increases with the increase of the dose of DZP co-administered with OXY. Similar results also happened between other opioids (buprenorphine and fentanyl) and benzodiazepines (alprazolam, midazolam, triazolam). Furthermore, we also verified that the minimal PBPK modeling can also be effective for some drugs and can sometimes replace full PBPK modeling when there is lack of information on PK parameters.

### **4.2 PHARMACODYNAMICS**

It is possible that there are additive PD interactions between opioids and benzodiazepines and benzodiazepines may be agonists or partial agonists for MOR and KOR since they show high binding affinities to the active conformations of these two receptors but relatively less binding affinities when binding to inactive conformations of MOR and KOR.

## APPENDIX

**Table S1 The input parameters for oxycodone and diazepam as well as their metabolites in full PBPK models.**

Parameters (Units)	oxycodone (S)	noroxycodone (M)	oxymorphone (M)	diazepam PO (I)	diazepam IV (I)	temazepam (M)	nordazepam (M)
Molecular weight (g/mol)	315.36	302.35	301.30	284.74	284.74	300.74	270.72
Log P <sub>o:w</sub>	1.40	0.202	0.900	2.82	2.82	2.19	2.79
pKa	8.28	8.50	8.20	3.40	3.40	3.40	3.40
B:P	1.3 [101]	0.90	1.01	0.59[102]	0.59	0.60	0.60
fu	0.60 [103]	0.89 (pred)	0.77 (pred)	0.030 [25, 104]	0.030	0.040 [105]	0.040
Ka	0.70 [71]			5.43 [pred]			
fa	0.6 [3]			1 [pred]			
Pe <sub>ff,man</sub> (10 <sup>-4</sup> cm/s)				12.43 [pred] (ADAM)			
V <sub>ss</sub> (L/kg)	6.17 (pred)	1.10 [106]	1.80 [106]	0.59 (pred)	0.59 (pred)	1.40 [107]	1.40
rhCYP3A4 CL <sub>int</sub> (μL/min/pmol)	0.055 [106]		0.130 [106]	0.214 [19, 24, 74, 75]	0.214	0.0043 [19, 24, 74, 75]	0.040 [19, 24, 74, 75]
rhCYP2D6 CL <sub>int</sub> (μL/min/pmol)	0.23 [106]	2.09 [106]					

rhCYP2C19				0.084	0.084		
CLint ( $\mu\text{L}/\text{min}/\text{pmol}$ )				[19, 24, 74, 75]			
Additional CL ( $\mu\text{L}/\text{min}/\text{mg}$ protein)	7.37 (pred)						
CLR (L/h)	8.1 [106]	21 [106]	21 [106]	0.10	0.10	4.0	4.0
Ki ( $\mu\text{M}$ )				1.65 (calc)	1.65		
Kapp ( $\mu\text{M}$ )				120 [30]	120		
Kinact (1/h)				7.8 [30]	7.8		

The values of molecular weight, Log  $P_{o:w}$  and pKa were all from PubChem database (<https://pubchem.ncbi.nlm.nih.gov/>). S represents substrate, M represents metabolite and I represents inhibitor. The PK value with ‘pred’ in parenthesis is the value predicted by Simcyp. The  $K_i$  value of diazepam with ‘calc’ was calculated by Equation 8.

**Table S2 The input parameters for oxycodone and diazepam as well as their metabolites in minimal PBPK models.**

Parameters (Units)	Oxycodone	noroxycodone	oxymorphone	diazepam	temazepam	Nordazepam
$F_{a,o/d}$	0.6 [103]			1		
$F_{g,o/d}$	1			1		
$K_{a,o/d}$ (1/h)	0.7 [71]			5.43 (Simcyp)		
$B:P$	1.3			0.59		
$f_{u,o/d}$	0.6 [103]			0.03		
$f_{b,o/d}$	0.46 (calc)			0.0508 (calc)		

$V_{GI}$ (L)	1.15 (Simcyp)			1.15 (Simcyp)		
$V_{pv}$ (L)	0.07 [44]			0.07 [44]		
$V_H$ (L)	1.65 (Simcyp)			1.65 (Simcyp)		
$V_{brain}$ (L)	1.45 [108]					
CLin (L/h)	150 [109]					
Clout (L/h)	50 [109]					
$V_{sys,o/d}$ (L)	180			35.8 (Simcyp)		
$Q_{pv,o/d}$ (L/h)	165			96 [110]		
$Q_{H,o/d}$ (L/h)	64 (Simcyp)			165		
CLint (L/h)	CLint,NOC: 32.06 CLint,OM: 7.83	CLint,NOC- NOM: 71.13	CLint,OM- NOM: 75.77	CLint,TMZ: 124.7 CLint,NDZ: 5	CLint,TMZ- OZP: 2.5	CLint,NDZ- OZP: 23.3
CLR (L/h)	8.1	21	21	0.1	4	4
Ki ( $\mu$ M)				1.65 (calc)		

The  $f_{b,o/d}$  was calculated from Equation 12. All intrinsic clearance was the same as the value of input parameters in Simcyp.

**Table S3 The input parameters for opioids and benzodiazepines as well as their metabolites in full PBPK models.**

Parameters (Units)	Buprenorphine (S)	Fentanyl (S)	Alprazolam (I)	Midazolam (I)	Triazolam (I)
Molecular weight (g/mol)	467.65	336.47	308.80	325.80	343.20
Log Po:w	4.98	4.00	2.12	2.53	2.42
pKa	9.62/8.31	8.77	2.4	10.95/6.2	10.52/2.91
B:P	0.55 [111]	1.119 [pred]	0.825	0.603	0.62

fu	0.07	0.16 [25]	0.29	0.032	0.179
Ka (1/h)	2		3.55	3.00	1.75
fa	0.3 [112]		1	1	1
V <sub>ss</sub> (L/kg)	5.18 [pred]	3.857 [pred]	0.76	0.88	0.48
rhCYP3A4 Clint ( $\mu\text{L}/\text{min}/\text{pmol}$ )		0.707 [113]		2.42 (1-OH); 0.16 (4-OH)	0.19 (1-OH); 0.06 (4-OH)
CYP3A4 Clint ( $\mu\text{L}/\text{min}/\text{mg}$ protein)			2.45		
rhCYP3A5 Clint ( $\mu\text{L}/\text{min}/\text{pmol}$ )				4.74 (1-OH); 0.12 (4-OH)	0.23 (1-OH); 0.067 (4-OH)
CYP3A5 Clint ( $\mu\text{L}/\text{min}/\text{mg}$ protein)			1.23		
CYP3A4 V <sub>max</sub> ( $\text{pmol}/\text{min}/\text{mg}$ protein)	10.4 [111]				
CYP3A4 k <sub>m</sub> ( $\mu\text{M}$ )	12.4 [111]				
CYP2C8 V <sub>max</sub> ( $\text{pmol}/\text{min}/\text{mg}$ protein)	1.4 [111]				
CYP2C8 k <sub>m</sub> ( $\mu\text{M}$ )	12.4 [111]				
rhUGT1A1 CLint ( $\mu\text{L}/\text{min}/\text{pmol}$ )	0.016 [111]				
rhUGT1A3 Clint ( $\mu\text{L}/\text{min}/\text{pmol}$ )	0.012 [111]				
rhUGT1A4 Clint ( $\mu\text{L}/\text{min}/\text{pmol}$ )				11.04	
rhUGT2B7 Clint ( $\mu\text{L}/\text{min}/\text{pmol}$ )	0.116 [111]				
CLR (L/h)		2.22 [113]	0.678	0.085	0.274
K <sub>i</sub> ( $\mu\text{M}$ )			1.63 (calc)	2.17 (calc)	1.02 (calc)

The values of molecular weight, Log P<sub>o.w</sub> and pK<sub>a</sub> were all from PubChem database (<https://pubchem.ncbi.nlm.nih.gov/>). S represents substrate, M represents metabolite and I

represents inhibitor. The PK value with 'pred' in parenthesis is the value predicted by Simcyp. The  $K_i$  value of diazepam with 'calc' was calculated by Equation 8. The PK parameters of alprazolam, midazolam and triazolam come for Simcyp database.

## BIBLIOGRAPHY

1. Ruhm, C.J., Drug involvement in fatal overdoses. *SSM - population health*, 2017. 3: p. 219-226.
2. Warner, M., et al., Drugs most frequently involved in drug overdose deaths: United States, 2010–2014. 2016.
3. Pöyhiä, R., A. Vainio, and E. Kalso, A review of oxycodone's clinical pharmacokinetics and pharmacodynamics. *Journal of Pain and Symptom Management*, 1993. 8(2): p. 63-67.
4. Jones, J.D., et al., Polydrug abuse: a review of opioid and benzodiazepine combination use. 2012. 125(1-2): p. 8-18.
5. Dart, R.C., et al., Trends in Opioid Analgesic Abuse and Mortality in the United States. *New England Journal of Medicine*, 2015. 372(3): p. 241-248.
6. Ruhm, C.J., Drug involvement in fatal overdoses. *SSM Popul Health*, 2017. 3: p. 219-226.
7. Olkkola, K. and J. Ahonen, Midazolam and other benzodiazepines, in *Modern Anesthetics*. 2008, Springer. p. 335-360.
8. Jones, C.M. and J.K.J.A.j.o.p.m. McAninch, Emergency department visits and overdose deaths from combined use of opioids and benzodiazepines. 2015. 49(4): p. 493-501.
9. Jones, J.D., S. Mogali, and S.D. Comer, Polydrug abuse: A review of opioid and benzodiazepine combination use. *Drug and Alcohol Dependence*, 2012. 125(1): p. 8-18.
10. Jann, M., W.K. Kennedy, and G.J.J.o.p.p. Lopez, Benzodiazepines: a major component in unintentional prescription drug overdoses with opioid analgesics. 2014. 27(1): p. 5-16.
11. Nielsen, S., D.A.J.D. Taylor, and a. dependence, The effect of buprenorphine and benzodiazepines on respiration in the rat. 2005. 79(1): p. 95-101.
12. Lintzeris, N., et al., Interactions on mixing diazepam with methadone or buprenorphine in maintenance patients. 2006. 26(3): p. 274-283.
13. Overdyk, F.J., et al., Association of opioids and sedatives with increased risk of in-hospital cardiopulmonary arrest from an administrative database. 2016. 11(2): p. e0150214.
14. Lee, S.C., et al., Comparison of toxicity associated with nonmedical use of benzodiazepines with buprenorphine or methadone. 2014. 138: p. 118-123.
15. Riley, J., et al., Oxycodone: a review of its use in the management of pain. *Current Medical Research and Opinion*, 2008. 24(1): p. 175-192.
16. Ordonez Gallego, A., M. Gonzalez Baron, and E. Espinosa Arranz, Oxycodone: a pharmacological and clinical review. *Clin Transl Oncol*, 2007. 9(5): p. 298-307.
17. Kalso, E., Oxycodone. *Journal of Pain and Symptom Management*, 2005. 29(5, Supplement): p. 47-56.
18. Lugo, R.A. and S.E. Kern, The Pharmacokinetics of Oxycodone. *Journal of Pain & Palliative Care Pharmacotherapy*, 2005. 18(4): p. 17-30.
19. Lalovic, B., et al., Quantitative contribution of CYP2D6 and CYP3A to oxycodone metabolism in human liver and intestinal microsomes. *Drug Metabolism and Disposition*, 2004. 32(4): p. 447.

20. Romand, S., et al., Characterization of oxycodone in vitro metabolism by human cytochromes P450 and UDP-glucuronosyltransferases. *Journal of Pharmaceutical and Biomedical Analysis*, 2017. 144: p. 129-137.
21. Olkkola, K.T. and N.M. Hagelberg, Oxycodone: new 'old' drug. *Curr Opin Anaesthesiol*, 2009. 22(4): p. 459-62.
22. Calcaterra, N.E. and J.C. Barrow, Classics in Chemical Neuroscience: Diazepam (Valium). *ACS Chemical Neuroscience*, 2014. 5(4): p. 253-260.
23. Lai, S.H., Y.J. Yao, and D.S.T. Lo, A survey of buprenorphine related deaths in Singapore. *Forensic Science International*, 2006. 162(1): p. 80-86.
24. Jung, F., et al., Diazepam Metabolism by DNA-Expressed Human 2C P450. *Drug Metabolism and Disposition*, 1997. 25(2): p. 133.
25. Goodman, L.S.L.S., Gilman, Alfred, Brunton, Laurence L. Lazo, John S. Parker, Keith L., Goodman & Gilman's the pharmacological basis of therapeutics, 11th. McGraw-Hill Medical Pub; 2006.
26. Mehta, A.K. and M.K. Ticku, An update on GABAA receptors. *Brain Research Reviews*, 1999. 29(2): p. 196-217.
27. Olsen, R.W. and A.J. Tobin, Molecular biology of GABAA receptors. *The FASEB Journal*, 1990. 4(5): p. 1469-1480.
28. Overholser, B.R. and D.R.J.T.A.j.o.m.c. Foster, Opioid pharmacokinetic drug-drug interactions. 2011. 17: p. S276-87.
29. Somogyi, A.A., et al., Pharmacogenetics of opioids. 2007. 81(3): p. 429-444.
30. Nishiya, Y., et al., Effects of organic solvents on the time-dependent inhibition of CYP3A4 by diazepam. *Xenobiotica*, 2010. 40(1): p. 1-8.
31. Iribarne, C., et al., Interaction of methadone with substrates of human hepatic cytochrome P450 3A4. *Toxicology*, 1997. 117(1): p. 13-23.
32. Spaulding, T.C., et al., The effect of diazepam on the metabolism of methadone by the liver of methadone-dependent rats. *Drug Metab Dispos*, 1974. 2(5): p. 458-63.
33. Chang, Y. and D.E. Moody, Effect of benzodiazepines on the metabolism of buprenorphine in human liver microsomes. *Eur J Clin Pharmacol*, 2005. 60(12): p. 875-81.
34. Lintzeris, N. and S. Nielsen, Benzodiazepines, methadone and buprenorphine: interactions and clinical management. *Am J Addict*, 2010. 19(1): p. 59-72.
35. Nims, R.W., et al., In vivo induction and in vitro inhibition of hepatic cytochrome P450 activity by the benzodiazepine anticonvulsants clonazepam and diazepam. *Drug Metab Dispos*, 1997. 25(6): p. 750-6.
36. Chang, Y. and D.E.J.E.j.o.c.p. Moody, Effect of benzodiazepines on the metabolism of buprenorphine in human liver microsomes. 2005. 60(12): p. 875-881.
37. Burrows, D.L., et al., A fatal drug interaction between oxycodone and clonazepam. 2003. 48(3): p. 683-686.
38. Stitzer, M.L., et al., Diazepam use among methadone maintenance patients: Patterns and dosages. *Drug and Alcohol Dependence*, 1981. 8(3): p. 189-199.
39. Lopez, C.F., et al., Programming biological models in Python using PySB. *Molecular Systems Biology*, 2013. 9.
40. Friesner, R.A., et al., Glide: a new approach for rapid, accurate docking and scoring. 1. Method and assessment of docking accuracy. *J Med Chem*, 2004. 47(7): p. 1739-49.

41. Wang, Z., et al., Comprehensive evaluation of ten docking programs on a diverse set of protein-ligand complexes: the prediction accuracy of sampling power and scoring power. *Phys Chem Chem Phys*, 2016. 18(18): p. 12964-75.
42. Glide User Manual. Schrodinger, Inc. New York, 2017.
43. Berg JM, T.J., Stryer L, The Michaelis-Menten Model Accounts for the Kinetic Properties of Many Enzymes., in *Biochemistry*. 5th edition, W.H. Freeman, Editor. 2002: New York.
44. Ito, K., et al., Prediction of the in vivo interaction between midazolam and macrolides based on in vitro studies using human liver microsomes *Drug Metabolism and Disposition*, 2003. 31(7): p. 945.
45. Davies, J.M., R.J. Poole, and D. Sanders, The computed free energy change of hydrolysis of inorganic pyrophosphate and ATP: apparent significance. for inorganic-pyrophosphate-driven reactions of intermediary metabolism. *Biochimica et Biophysica Acta (BBA) - Bioenergetics*, 1993. 1141(1): p. 29-36.
46. Marzolini, C., et al., Physiologically Based Pharmacokinetic Modeling to Predict Drug-Drug Interactions with Efavirenz Involving Simultaneous Inducing and Inhibitory Effects on Cytochromes. *Clin Pharmacokinet*, 2017. 56(4): p. 409-420.
47. Budha, N.R., et al., Evaluation of Cytochrome P450 3A4-Mediated Drug-Drug Interaction Potential for Cobimetinib Using Physiologically Based Pharmacokinetic Modeling and Simulation. *Clin Pharmacokinet*, 2016. 55(11): p. 1435-1445.
48. Jamei, M., et al., A Mechanistic Framework for In Vitro–In Vivo Extrapolation of Liver Membrane Transporters: Prediction of Drug–Drug Interaction Between Rosuvastatin and Cyclosporine. Vol. 53. 2013.
49. Kostewicz, E.S., et al., PBPK models for the prediction of in vivo performance of oral dosage forms. *European Journal of Pharmaceutical Sciences*, 2014. 57: p. 300-321.
50. Zhou, S., et al., Mechanism-based inhibition of cytochrome P450 3A4 by therapeutic drugs. *Clin Pharmacokinet*, 2005. 44(3): p. 279-304.
51. Grillo, J.A., et al., Utility of a physiologically-based pharmacokinetic (PBPK) modeling approach to quantitatively predict a complex drug-drug-disease interaction scenario for rivaroxaban during the drug review process: implications for clinical practice. *Biopharm Drug Dispos*, 2012. 33(2): p. 99-110.
52. Nestorov, I.A., et al., Lumping of Whole-Body Physiologically Based Pharmacokinetic Models. *Journal of Pharmacokinetics and Biopharmaceutics*, 1998. 26(1): p. 21-46.
53. Jo, S., et al., CHARMM-GUI: a web-based graphical user interface for CHARMM. *J Comput Chem*, 2008. 29(11): p. 1859-65.
54. Jorgensen, W.L., et al., Comparison of simple potential functions for simulating liquid water. *The Journal of Chemical Physics*, 1983. 79(2): p. 926-935.
55. Wang, J., et al., Development and testing of a general amber force field. *J Comput Chem*, 2004. 25(9): p. 1157-74.
56. Bayly, C.I., et al., A well-behaved electrostatic potential based method using charge restraints for deriving atomic charges: the RESP model. *The Journal of Physical Chemistry*, 1993. 97(40): p. 10269-10280.
57. Frisch, M.J., et al., Gaussian 16 Rev. B.01. 2016: Wallingford, CT.
58. Wang, J., et al., Automatic atom type and bond type perception in molecular mechanical calculations. *J Mol Graph Model*, 2006. 25(2): p. 247-60.

59. Case, D.A., Betz RM, Cerutti DS et al, AMBER 2016. University of California, San Francisco, 2016.
60. Gotz, A.W., et al., Routine Microsecond Molecular Dynamics Simulations with AMBER on GPUs. 1. Generalized Born. *J Chem Theory Comput*, 2012. 8(5): p. 1542-1555.
61. Salomon-Ferrer, R., et al., Routine Microsecond Molecular Dynamics Simulations with AMBER on GPUs. 2. Explicit Solvent Particle Mesh Ewald. *J Chem Theory Comput*, 2013. 9(9): p. 3878-88.
62. Izaguirre, J.A., et al., Langevin stabilization of molecular dynamics. *The Journal of Chemical Physics*, 2001. 114(5): p. 2090-2098.
63. Ryckaert, J.-P., G. Ciccotti, and H.J.C. Berendsen, Numerical integration of the cartesian equations of motion of a system with constraints: molecular dynamics of n-alkanes. *Journal of Computational Physics*, 1977. 23(3): p. 327-341.
64. Hou, T., et al., Assessing the Performance of the MM/PBSA and MM/GBSA Methods. 1. The Accuracy of Binding Free Energy Calculations Based on Molecular Dynamics Simulations. *Journal of Chemical Information and Modeling*, 2011. 51(1): p. 69-82.
65. Rocchia, W., E. Alexov, and B. Honig, Extending the Applicability of the Nonlinear Poisson–Boltzmann Equation: Multiple Dielectric Constants and Multivalent Ions. *The Journal of Physical Chemistry B*, 2001. 105(28): p. 6507-6514.
66. Xu, L., et al., Assessing the Performance of MM/PBSA and MM/GBSA Methods. 3. The Impact of Force Fields and Ligand Charge Models. *The Journal of Physical Chemistry B*, 2013. 117(28): p. 8408-8421.
67. Lavecchia, A., et al., Modeling of Cdc25B Dual Specificity Protein Phosphatase Inhibitors: Docking of Ligands and Enzymatic Inhibition Mechanism. Vol. 1. 2006. 540-50.
68. Hillestad, L., et al., Diazepam metabolism in normal man. *Clinical Pharmacology & Therapeutics*, 1974. 16(3part1): p. 479-484.
69. Johanson, C.E. and E.H. Uhlenhuth, Drug preference and mood in humans: Diazepam. *Psychopharmacology*, 1980. 71(3): p. 269-273.
70. Welling, P.G., *Pharmacokinetics : processes, mathematics, and applications*(2nd ed). 1997, Washington, D.C: American Chemical Society.
71. Li, Y., et al., Slow drug delivery decreased total body clearance and altered bioavailability of immediate- and controlled-release oxycodone formulations. *Pharmacology Research & Perspectives*, 2016. 4(1): p. e00210.
72. Molina, D.K. and V.J. DiMaio, Normal organ weights in men: part II-the brain, lungs, liver, spleen, and kidneys. *Am J Forensic Med Pathol*, 2012. 33(4): p. 368-72.
73. Suzuki, K., et al., Quantitative radiology: automated CT liver volumetry compared with interactive volumetry and manual volumetry. *AJR. American journal of roentgenology*, 2011. 197(4): p. W706-W712.
74. Kenworthy, K.E., et al., Multisite Kinetic Models for CYP3A4: Simultaneous Activation and Inhibition of Diazepam and Testosterone Metabolism. *Drug Metabolism and Disposition*, 2001. 29(12): p. 1644.
75. Shou, M., et al., Sigmoidal kinetic model for two co-operative substrate-binding sites in a cytochrome P450 3A4 active site: an example of the metabolism of diazepam and its derivatives. *The Biochemical journal*, 1999. 340 ( Pt 3)(Pt 3): p. 845-853.
76. Divoll, M., et al., Benzodiazepine overdose: plasma concentrations and clinical outcome. *Psychopharmacology (Berl)*, 1981. 73(4): p. 381-3.

77. Moody, D.E., Drug Interactions with Benzodiazepines: Epidemiologic Correlates with Other CNS Depressants and In Vitro Correlates with Inhibitors and Inducers of Cytochrome P450 3A4, in Handbook of Drug Interactions: A Clinical and Forensic Guide, A. Mozayani and L. Raymon, Editors. 2012, Humana Press: Totowa, NJ. p. 25-116.
78. Park, T.W., et al., Benzodiazepine prescribing patterns and deaths from drug overdose among US veterans receiving opioid analgesics: case-cohort study. *BMJ : British Medical Journal*, 2015. 350.
79. Raffa, R.B. and J.V. Pergolizzi, Jr., Opioid formulations designed to resist/deter abuse. *Drugs*, 2010. 70: p. 1657+.
80. Friedman, H., et al., Pharmacokinetics and pharmacodynamics of oral diazepam: effect of dose, plasma concentration, and time. *Clin Pharmacol Ther*, 1992. 52(2): p. 139-50.
81. Klotz, U., et al., The effects of age and liver disease on the disposition and elimination of diazepam in adult man. *The Journal of clinical investigation*, 1975. 55(2): p. 347-359.
82. Tang, J., et al., In vitro metabolism of fipronil by human and rat cytochrome P450 and its interactions with testosterone and diazepam. *Chemico-Biological Interactions*, 2004. 147(3): p. 319-329.
83. Kuhlman, J.J., Jr., et al., Human Pharmacokinetics of Intravenous, Sublingual, and Buccal Buprenorphine\*. *Journal of Analytical Toxicology*, 1996. 20(6): p. 369-378.
84. Shankaran, H., F. Adeshina, and J.G. Teegarden, Physiologically-based pharmacokinetic model for Fentanyl in support of the development of Provisional Advisory Levels. *Toxicol Appl Pharmacol*, 2013. 273(3): p. 464-76.
85. Donovan, J.L., et al., Siberian ginseng (*Eleutherococcus senticosus*) effects on CYP2D6 and CYP3A4 activity in normal volunteers. *Drug Metab Dispos*, 2003. 31(5): p. 519-22.
86. Qiu, F., et al., Opposite Effects of Single-Dose and Multidose Administration of the Ethanol Extract of Danshen on CYP3A in Healthy Volunteers. *Evid Based Complement Alternat Med*, 2013. 2013: p. 730734.
87. Greenblatt, D.J., et al., Sensitivity to Triazolam in the Elderly. *New England Journal of Medicine*, 1991. 324(24): p. 1691-1698.
88. Wolf, B.C., et al., One hundred seventy two deaths involving the use of oxycodone in Palm Beach County. *J Forensic Sci*, 2005. 50(1): p. 192-5.
89. Greenblatt, D.J., et al., Rapid Recovery From Massive Diazepam Overdose. *JAMA*, 1978. 240(17): p. 1872-1874.
90. Bostrom, E., M. Hammarlund-Udenaes, and U.S. Simonsson, Blood-brain barrier transport helps to explain discrepancies in in vivo potency between oxycodone and morphine. *Anesthesiology*, 2008. 108(3): p. 495-505.
91. Lawrence, I.K.L., A Concordance Correlation Coefficient to Evaluate Reproducibility. *Biometrics*, 1989. 45(1): p. 255-268.
92. Lewis, J.W., Buprenorphine. *Drug and Alcohol Dependence*, 1985. 14(3): p. 363-372.
93. Leander, J.D., Buprenorphine has potent kappa opioid receptor antagonist activity. *Neuropharmacology*, 1987. 26(9): p. 1445-1447.
94. Mellar P. Davis, P.A.G., Janet Hardy, and Columba Quigley, *Opioids in Cancer Pain* (2 ed.). 2013: Oxford University Press.
95. Niciu, M.J. and A.J. Arias, Targeted opioid receptor antagonists in the treatment of alcohol use disorders. *CNS drugs*, 2013. 27(10): p. 777-787.

96. Cox, R.F. and M.A. Collins, The effects of benzodiazepines on human opioid receptor binding and function. *Anesth Analg*, 2001. 93(2): p. 354-8 , 3rd contents page.
97. Spetea, M., et al., Effect of a 6-cyano substituent in 14-oxygenated N-methylmorphinans on opioid receptor binding and antinociceptive potency. *J Med Chem*, 2005. 48(15): p. 5052-5.
98. Kumar, V., et al., Selectively promiscuous opioid ligands: discovery of high affinity/low efficacy opioid ligands with substantial nociceptin opioid peptide receptor affinity. *Journal of medicinal chemistry*, 2014. 57(10): p. 4049-4057.
99. Lattin, D.L., et al., Synthesis of analogues of acetylmethadol and methadol as potential narcotic antagonists. *J Med Chem*, 1981. 24(7): p. 903-6.
100. Stavitskaya, L., et al., Deconstructing 14-phenylpropyloxymetopon: minimal requirements for binding to mu opioid receptors. *Bioorg Med Chem*, 2012. 20(14): p. 4556-63.
101. Moore, C., T. Kelley-Baker, and J. Lacey, Interpretation of oxycodone concentrations in oral fluid. *J Opioid Manag*, 2012. 8(3): p. 161-6.
102. Jones, A.W. and H. Larsson, Distribution of diazepam and nordiazepam between plasma and whole blood and the influence of hematocrit. *Ther Drug Monit*, 2004. 26(4): p. 380-5.
103. Seaton, S., M. Reeves, and S. McLean, Oxycodone as a component of multimodal analgesia for lactating mothers after Caesarean section: Relationships between maternal plasma, breast milk and neonatal plasma levels. *Australian and New Zealand Journal of Obstetrics and Gynaecology*, 2007. 47(3): p. 181-185.
104. Mandelli, M., G. Tognoni, and S. Garattini, Clinical Pharmacokinetics of Diazepam. *Clinical Pharmacokinetics*, 1978. 3(1): p. 72-91.
105. Chin, P.K.L., et al., Adult age and ex vivo protein binding of lorazepam, oxazepam and temazepam in healthy subjects. *British journal of clinical pharmacology*, 2011. 72(6): p. 985-989.
106. Marsousi, N., et al., Prediction of Metabolic Interactions With Oxycodone via CYP2D6 and CYP3A Inhibition Using a Physiologically Based Pharmacokinetic Model. *CPT: pharmacometrics & systems pharmacology*, 2014. 3(12): p. e152-e152.
107. Divoll, M., et al., Effect of age and gender on disposition of temazepam. *Journal of Pharmaceutical Sciences*, 1981. 70(10): p. 1104-1107.
108. Keller, S.S. and N. Roberts, Measurement of brain volume using MRI: software, techniques, choices and prerequisites. *J Anthropol Sci*, 2009. 87: p. 127-51.
109. Boström, E., U.S.H. Simonsson, and M. Hammarlund-Udenaes, In Vivo Blood-Brain Barrier Transport of Oxycodone in the Rat: Indications for Active Influx and Implications for Pharmacokinetics/Pharmacodynamics. *Drug Metabolism and Disposition*, 2006. 34(9): p. 1624.
110. Ito, K., et al., Prediction of the in vivo interaction between midazolam and macrolides based on in vitro studies using human liver microsomes. *Drug Metab Dispos*, 2003. 31(7): p. 945-54.
111. Kalluri, H.V., et al., A physiologically based pharmacokinetic modelling approach to predict buprenorphine pharmacokinetics following intravenous and sublingual administration. *British Journal of Clinical Pharmacology*, 2017. 83(11): p. 2458-2473.
112. Mendelson, J., et al., Bioavailability of Sublingual Buprenorphine. *The Journal of Clinical Pharmacology*, 1997. 37(1): p. 31-37.

113. Encinas, E., et al., A predictive pharmacokinetic/pharmacodynamic model of fentanyl for analgesia/sedation in neonates based on a semi-physiologic approach. *Paediatr Drugs*, 2013. 15(3): p. 247-57.